Impacts of reductions in non-methane short-lived climate forcers on future climate extremes and the resulting population exposure risks in eastern and southern Asia

Yingfang Li[1], Zhili Wang[1*], Yadong Lei[1], Huizheng Che[1], Xiaoye Zhang[1]

[1]State Key Laboratory of Severe Weather and Key Laboratory of Atmospheric Chemistry of CMA, Chinese Academy of Meteorological Sciences, Beijing, 100081, China

Correspondence to: Zhili Wang (wangzl@cma.gov.cn)

Abstract. Non-methane short-lived climate forcers (SLCFs), including aerosols, ozone, and their precursors, are important climate forcings and primary air pollutants. Future stringent SLCF emissions controls to mitigate air pollution will substantially impact regional climate change. Here, we investigate the changes in future climate extremes and resulting population exposure risks in Asia during 2031–2050 in response to non-methane SLCF emissions reductions using multi-model ensemble (MME) simulations under two shared socioeconomic pathway (SSP) scenarios (SSP3-7.0 and SSP3-7.0-lowNTCF) with different air quality control measures from the Aerosol and Chemistry Model Intercomparison Project (AerChemMIP), which is endorsed by Coupled Model Intercomparison Project phase 6 (CMIP6). The MME results show that future reductions in non-methane SLCF emissions lead to an increase of 0.23 ± 0.16 W m^{-2} in global annual mean effective radiative forcing, thereby magnifying the greenhouse gas (GHG)-induced global surface warming by 0.19 ± 0.1 K during 2031–2050. In terms of the entire study area, the additional warming caused by the non-methane SLCF reductions increases the hottest days (TXx) by 0.3 ± 0.1 K, the percentage of warm days (TX90p) by 4.8 ± 2.2 %, the number of tropical nights (TR) by 1.7 ± 0.8 days, the warm spell duration (WSDI) by 1.0 ± 0.4 days, the number of heavy precipitation days (R10) by 1.0 ± 0.5 days, the maximum consecutive 5-day precipitation (RX5day) by 1.0 ± 0.3 mm, and the total wet-day precipitation (R95p) by 16.4 ± 7.3 mm during 2031–2050. For temperature extremes, the largest regional increases of TXx, TX90p, and WSDI occur in northern India (NIN) and northern China (NC). Relatively large increases in TR are projected in NC and the Sichuan Basin (SCB), reaching 5.1 ± 2.5 days and 4.9 ± 3.3 days, respectively. For precipitation extremes, the regional changes are greatest in southern China (SC), particularly southwestern China (SWC), where reductions of non-methane SLCF emissions increases R10 by 2.5 ± 1.9 days, RX5day by 2.5 ± 1.5 mm, and R95p by 37.5 ± 22.6 mm. Moreover, the populations exposed to temperature and precipitation extremes increase most sharply in NIN, reaching (32.2 ± 11.4) × 10^7 person-days and (4.6 ± 6.1) × 10^6 person-days during 2031–2050, respectively, followed by NC and SCB. Our results highlight the significant impacts of non-methane SLCF reductions on future climate extremes and related exposure risks in eastern and southern Asia, which are comparable to the impact associated with increased GHG forcing in some regions.

1 Introduction

Short-lived climate forcers (SLCFs), also known as near-term climate forcers (NTCFs), include aerosols (e.g., sulfates, black carbon (BC), organic carbon (OC), ammonium salts, and nitrate), ozone, methane (CH_4), and their precursors (e.g., sulfur dioxide (SO_2), nitrogen oxides (NOx), carbon monoxide (CO), and ammonia) (Myhre et al., 2013). Since the beginning of the industrial era, human activities have led to a significant increase in emissions of SLCFs (Hoesly et al., 2018). Non-methane SLCFs, including aerosols, ozone, and their precursors, affect not only climate but also air quality. Previous studies have revealed significant influences of non-methane SLCFs on global and regional climate as well as human health (Liao et al., 2015; Forster et al., 2021; Apte et al., 2015; Malley et al., 2017; Xie et al., 2016a).

Increasing and accumulating GHGs emissions from human activities since the industrial revolution are the main drivers of global warming, but care must be taken in attributing an acceleration in human-induced global warming to these changes in SLCFs emissions (Jenkins et al., 2022). According to the Sixth Assessment Report of the Intergovernmental Panel on Climate Change (IPCC, AR6), global average effective radiative forcing (ERF) since the beginning of the industrial revolution (1750–2019) is –1.1 (–1.7 to –0.4) W m^{-2} for aerosols and +0.47 (+0.24 to +0.71) W m^{-2} for ozone (Forster et al., 2021). Over the past few decades, climate change caused by non-methane SLCFs has had an important impact on natural ecosystems and human societies in Asia (Ramanathan et al., 2007; Li et al., 2016). North-East of India witnessed cooler maximum temperatures due to increased aerosols (Freychet et al. 2019). Surface cooling and tropospheric atmospheric thermal responses associated with aerosol forcing can weaken the East Asian summer monsoon, thereby suppressing precipitation in the East Asian monsoon region (Li et al., 2016; Xie et al., 2016b; Wang et al., 2019, 2020; Mu and Wang, 2021). The increase in aerosols since the 1950s may have led to weakening of summer precipitation in South Asia (Bollasina et al., 2011) and the anomalous precipitation pattern described as "southern flood/northern drought" in eastern China (Li et al., 2016). Regional aerosol-cloud interactions may be the main factor causing extreme precipitation variability in India and China during 1979–2005 (Lin et al., 2018). In terms of ozone, Chang et al. (2009) noted that tropospheric ozone increased average surface air temperature (SAT) by 0.43 ℃ and decreased average precipitation by 0.08 mm day^{-1} in eastern China during 1971–2000. The simulation results of Li et al. (2018) showed that East Asian summer monsoon circulation was enhanced over southern China but weakened over northern China during 2001–2010 due to tropospheric ozone forcing.

Emissions controls implemented by governments, which aim to mitigate global warming and improve air quality, have led to significant changes in non-methane SLCF emissions that will affect future climate change (Naik et a., 2021). Meanwhile, the important role of non-methane SLCFs in historical climate change in Asia (Bollasina et al., 2011; Dong et al., 2019; Wang et al., 2019) suggests that SLCF emissions reductions may have major implications for future regional climate and its extremes (Wang et al., 2016; Zhang et al., 2018; Wilcox et al., 2020). In previous research, Turnock et el. (2020) made a first assessment of historical and future changes in air pollutants and Zanis et el. (2022) presented an analysis of the effect of climate change on surface ozone discussing the related penalties and benefits around the globe using the five Earth system models (ESMs) from the Coupled Model Intercomparison Project phase 6 (CMIP6). But the assessed impact of reducing non-methane SLCF emissions on future climate change has been limited to the effect of aerosol forcing associated with incomplete interactive tropospheric chemistry schemes in global climate models. Future aerosol emissions reductions could greatly aggravate the warming effect caused by greenhouse gas (GHG) forcing (Lin et al., 2016; Hienola et al., 2018), particularly in eastern and southern Asia, and may increase surface temperatures by 0.5 ℃ in some regions (Westervelt et al., 2015; Chuwah et al., 2016) and cause a significant increase in extreme high-temperature events (Wang et al., 2016; Samset et al., 2018; Luo et al., 2020). In eastern Asia, under global warming 1.5 ℃ and 2 ℃, China is expected to grow at a faster rate than the global mean, and there is a strong warming in the Tibetan Plateau and when studying changes in local climate between 1.5 ℃ and 2 ℃ of global warming, non-GHGs influences need to be considered (King et al. 2018; You et al. 2020). The effect of projected reductions in anthropogenic aerosol emissions over eastern Asia caused an increase in summer temperatures and raised the likelihood of extreme hot summers (King et al. 2018). Future aerosol reductions may also shift the tropical rain belt northwards, enhancing precipitation in the Asian monsoon region (Westervelt et al., 2018; Zanis et al., 2020) and shifting both the mean and extreme values of precipitation toward larger values (Zhao et al., 2018). Asia is a region where extreme precipitation is particularly sensitive to aerosol reductions (Lin et al., 2016; Samset et al., 2018).

The precursors of aerosols and ozone are homologous and overlapping (e.g., NOx, volatile organic compounds (VOCs)) (Myhre et al., 2013). Implementation of air pollution control measures inevitably causes simultaneous changes in their radiative forcings. Therefore, considering the impacts of changes in non-methane SLCFs on future climate, particularly on regional extreme climate events, is essential. However, few studies in this field have been conducted to date. A recent study considering emissions reductions of aerosols, ozone, and their precursors showed that future non-methane SLCF reductions will not only improve air quality but also increase global mean temperature, precipitation, and climate extremes in the mid-21st century, with more marked warming and wetting trends in some regions, particularly Asia and the Arctic (Allen et al., 2020). However, there were some limitations in that study. First, Allen et al. (2020) only considered three extreme indicators including hottest day, wettest day, and consecutive dry days to examine the effects of future non-methane SLCF reductions on climate extremes. These three indicators were not enough to represent climate extremes, especially the lack of some indicators related to human health. For example, tropical night (TR) usually occurs in combination with extended periods of heat (particularly in extra-tropical regions) and have been suggested to be problematic for human health (Weisskopf et al., 2002; Patz et al., 2005) and the maximum consecutive 5-day precipitation (RX5day) can be used as an indicator of flooding and related hazards (Frich et al., 2002; Sillmann et al., 2013). Second, climate extremes pose a serious threat on human body (Bras et al., 2021; Tellman et al., 2021). Quantifying avoided population exposure to climate extremes associated with future non-methane SLCF reductions is valuable for future policymaking on climate change mitigation and adaptation, especially in these densely populated and industrially developed regions of Asia, which is lacked in Allen et al. (2020).

With the continued global warming caused by GHG emissions, the frequency of climate extremes increases (Zhou and Qian, 2019), increasing the threat to human health, economic stability, and environmental sustainability. As a densely populated and climate-vulnerable region, Asia is at high risk for future population exposure to climate extremes. In the coming decades, the population exposed to extreme heat in East Asia will continue to increase under most future scenarios

(An et al., 2020). The population exposure to extreme precipitation over the Indus River Basin is projected to increase by 72.4%, 122.7%, and 87.6%, respectively, with global warming of 1.5 ℃, 2.0 ℃, and 3.0 ℃ (Zhao et al., 2021). The population affected by extreme precipitation in China is projected to increase by nearly 22% by the end of the 21st century under the representative concentration pathway–shared socioeconomic pathway (RCP-SSP) scenario RCP4.5-SSP2, with the largest absolute increase in eastern China (Chen and Sun, 2020). With increasing warming in the future, dry conditions across China will be further aggravated, and an additional 12.9 million people will be exposed to droughts under the 1.5 ℃ global warming scenario (Chen et al., 2018; Chen and Sun, 2019). This raises the issue of whether reductions in non-methane SLCF emissions will further exacerbate the intensity and frequency of extreme climate events and the resulting risk of population exposure.

With continuous development, some climate system models have become more complete ESMs, which consider the coupling of Earth system processes and support relatively realistic and complete analysis of the whole Earth-atmosphere system. Furthermore, the Aerosols and Chemistry Intercomparison Project (AerChemMIP) was established by the CMIP6 to comprehensively assess the impacts of SLCFs on climate and air quality (Collins et al., 2017), which can further elucidate changes in atmospheric chemical composition and their interactions with changes in global and regional climate. Here, we quantify the impacts of non-methane SLCF emissions reductions on extreme climate changes and the resulting population exposure risks during 2031–2050 in eastern and southern Asia using historical simulations and two scenario simulations (SSP3-7.0 and SSP3-7.0-lowNTCF) with state-of-the-art ESMs from the AerChemMIP (Collins et al., 2017). The scope of eastern and southern Asia in this study is defined as 0-60 °N, 70-150 °E.

The remainder of this paper is organized as follows. Section 2 describes the models, simulations, and calculations of climate extremes and related population exposure. Section 3 contains the results. Finally, our discussion and conclusions are presented in Section 4.

2 Methods

2.1 Future emissions scenarios

Simulations under two AerChemMIP scenarios, SSP3-7.0 and SSP3-7.0-lowNTCF, were performed to assess the impacts of non-methane SLCF changes on climate and air quality (Collins et al., 2017; Allen et al., 2020). The SSP3-7.0 scenario is used as the reference scenario (~7.0 W m^{-2} at 2100), as it includes no climate policies related to GHG reductions and weak air pollution controls. In this scenario, the future climate change is approximatively influenced by GHG forcing only. The perturbation scenario SSP3-7.0-lowNTCF uses the same GHG forcing path but with strong air pollution controls, and thus future climate change in this scenario is influenced by a combination of GHG forcing and reduction of non-methane SLCF emissions. As shown in Figure 1, the two simulations include the same variation in carbon dioxide (CO_2) and CH_4, both of which continue to increase in the future. However, non-methane SLCFs exhibit different changes in these two scenarios. Global emissions of non-methane SLCFs are maintained at a stable level or vary slightly after 2020 under the

SSP3-7.0 scenario, with a decrease of 1% in SO_2 and increases of 7–13% in other SLFCs by 2050. Global emissions of all non-methane SLCFs show significant downward trends under the SSP3-7.0-lowNTCF scenario, ranging from 10% for BC to 55% for SO_2 by 2050. Assuming that the joint impact of GHGs and non-methane SLCFs are approximated as a linear superposition of their respective impacts, the impact of non-methane SLCF mitigation can be quantified as the difference between the results of simulation under the two scenarios (SSP3-7.0-lowNTCF minus SSP3-7.0) (Allen et al., 2020).

2.2 Models and simulations

Seven CMIP6 ESMs with interactive representation of tropospheric aerosols and atmospheric chemistry were used to conduct the SSP3-7.0 and SSP3-7.0-lowNTCF simulations (Table 1), with integration periods of 2015–2055 and individual models integrated through 2100. We used the daily and monthly outputs for both scenarios from 2015 to 2050. Historical climate simulations (Historical) for 1995–2014 from the same models were used as the reference period. In addition to coupled ocean-atmosphere simulations, these models were also used for Atmospheric Model Intercomparison Project (AMIP)-style simulations with the time-varying sea surface temperature (SST) outputs from SSP3-7.0 simulations under the two emissions scenarios to quantify the ERF associated with future changes in atmospheric composition (Collins et al., 2017). ERF is a measure of the extent to which forcing agents affect climate, defined as the change in net radiative flux at the top of the atmosphere caused by a disturbance that allows for changes in atmospheric temperature, water vapor, and clouds, but keeps global SST unchanged (Myhre et al., 2013; Forster et al., 2016; Pincus et al., 2016). At present, there are few models carrying out both SSP3-7.0 and SSP3-7.0-lowNTCF experiments, thus, we directly used the CMIP6 multi-model ensemble (MME) mean to investigate the changes of climate extremes in response to future SLCFs emission reductions.

To evaluate the performance of the models, a gridded daily maximum and minimum temperature and daily precipitation dataset obtained from the National Oceanic and Atmospheric Administration (NOAA) Climate Prediction Center (CPC) is used here. This dataset was constructed using optimal interpolation methods based on approximately 16,000 station and satellite observations (Chen et al., 2020b). It spans the period from 1979 to the present and has a high level of resolution of $0.5° \times 0.5°$. All model outputs as well as observations were interpolated into a common grid ($1° \times 1°$) through bilinear interpolation except precipitation data, which used first-order conservative interpolation.

We compared the simulated results with the observational climate extremes during 1995–2014 (Fig. 2). In general, the CMIP6 MME can reasonably reproduce the observed spatial distribution of extreme temperature and precipitation indices. For the extreme temperature indices, the maximums obtained from both the CMIP6 MME and observations are found in eastern China and southern Asia, especially for the simulated absolute extreme indices (TXx, TR) (Figs. 2a, 2b, 2e and 2f), which are generally consistent with the observations in spatial distribution with limited difference in magnitude. Relative to the absolute extreme indices, the percentile and duration indices show large differences between the CMIP6 MME and observation (Figs. 2c, 2d, 2g and 2h). Previous studies also shown that both CMIP5 and CMIP6 perform relatively unsatisfactorily in simulating spatial patterns of the duration and percentile indices (Fan et al., 2020; Guo et al., 2021). For R10, RX5day and R95p, the climatological mean is well captured by CMIP6 MME, although it tends to produce overestimates especially over southeastern Qinghai-Tibet Plateau and the Indo-China Peninsula (Figs. 2i-n). In addition, the CMIP6 MME underestimates the CDD in northwest China and along Mongolia (Figs. 2o and 2p), which is consistent with previous studies (Zhu et al., 2021; Kim et al., 2020). Although the CMIP6 MME produce some regional biases with respect to observation, such biases will be significantly reduced when considering the difference between the two segments of time (Sillmann et al., 2013; Chen et al., 2020). In this study, we focused on the changes in the future (2031–2050) relative to the reference period (1995–2014), so the results of the CMIP6 MME can be considered representative.

2.3 Climate extremes indices

Following the definitions of the Expert Team for Climate Change Detection and Indices, six extreme temperature indices and four extreme precipitation indices representing intensity and frequency were employed in this study (Table 2). Due to incomplete data provided by CESM2-WACCM and GISS-E2-1-G, the extreme temperature indices were calculated with the remaining five models, and the extreme precipitation indices were calculated with the six models other than GISS-E2-1-G. We focused on the changes in extreme climate indices in the future (2031–2050) relative to the reference period (1995–2014).

2.4 Population exposure

Population exposure to climate extremes can be estimated by multiplying the frequency of extreme events by the number of people, and this method has been widely employed to assess future climate risks (Jones et al., 2015). Gridded population datasets for 2000 and 2040 under SSP3 were used to represent the population during the reference and future periods, respectively (Jones and Oneill 2016). These population datasets were summed for each grid box of $1° \times 1°$ to match the resolution of the climate data.

Population exposures to extreme heat and heavy precipitation were are calculated as the population exposed multiplied by the number of days with a daily maximum temperature greater than the 90th percentile of the reference period and by the number of days with daily precipitation greater than the 95th percentile of the reference period, respectively (Chen et al., 2020; Sun et al., 2022). The exposure change (Δexpo) could be decomposed into three parts, namely, changes driven by the climate effect, the population effect, and their interaction:

$$\Delta expo = (c + \Delta c) \cdot (p + \Delta p) - c \cdot p = c \cdot \Delta p + p \cdot \Delta c + \Delta c \cdot \Delta p \ , \qquad (1)$$

where c and p are the number of extreme days and population in the baseline period, respectively. Δc and Δp are the changes in climate extreme days and population in the future with respect to the baseline period. Thus, the terms of $c \cdot \Delta p$, $p \cdot \Delta c$, and $\Delta c \cdot \Delta p$ represent the population, climate, and population-climate interaction effects, respectively, on exposure changes, allowing for attribution analysis of changes in population exposure.

3 Results

3.1 Changes in global ERF and SAT

Figure 2 shows the spatial patterns of ERF under the SSP3-7.0 and SSP3-7.0-lowNTCF scenarios and their changes associated with reductions in non-methane SLCF emissions during 2031–2050 relative to 1995–2014. As GHG concentrations increase and SLCF concentrations decrease, more long-wave radiation is absorbed and less short-wave radiation is reflected, resulting in positive global average ERF values under both scenarios (Fig. 2a and b). Non-methane SLCF emissions reductions lead to positive ERF over most of the globe, particularly in the Northern Hemisphere (Fig. 2c). Increases in ERF of approximately 1 W m^{-2} occur mainly in Eurasia north of 40°N, the northern Pacific Ocean, northern America, and the northern Atlantic Ocean. The largest increases of more than 1.5 W m^{-2} are found over India, southeastern Asia, and surrounding oceans (Fig. 2c). Notably, some negative ERFs remain over northern China, the Sichuan Basin, Arabian Peninsula, and northern Africa, as the increase in low cloud cover induced by changes in regional precursor concentrations leads to greater reflection of shortwave radiation (Yang et al., 2017; Zhang et al., 2018). The multi-model ensemble (MME) global annual mean ERF induced by non-methane SLCF emissions reductions is +0.23 W m^{-2}, with positive values obtained from all models except GFDL-ESM4 (Table 3).

Figure 3 shows the MME global changes in SAT under each scenario. Increases in SATs occur worldwide during 2031–2050 under both the SSP3-7.0 and SSP3-7.0-lowNTCF scenarios (Fig. 3a and b). The SAT increases are greater in the Northern Hemisphere and on land than in the Southern Hemisphere and ocean areas due to greater precursor emissions in the Northern Hemisphere and the high heat capacity of the ocean. Regionally, the greatest warming of more than 1.5 K is found in central and northern Asia and in northern North America, particularly in the Arctic, where warming is greater than 2.5 K. Moreover, such warming is exacerbated by future non-methane SLCF emissions reductions in most regions of the world, particularly in the Northern Hemisphere (Fig. 3c). Previous studies have shown that reduction of sulfate aerosols is the dominant driver of future SAT increases in response to aerosol forcing, particularly in the Northern Hemisphere (Baker et al., 2015; Samset et al., 2018). Future reductions in non-methane SLCF emissions causes additional warming of more than 0.2 K throughout Eurasia, the northern Pacific, and northern North America. In particular, warming in the Arctic will exceed 0.6 K (Fig. 3c). The reduction of non-methane SLCF emissions results in an average increase of 0.19 K in global mean SAT in the MME results, ranging from 0.06 K to 0.29 K across different models (Table 3). Furthermore, the increase in global mean SAT is consistent with the increase in global mean ERF except for GFDL-ESM4. However, warming and positive ERF do not correspond exactly in some regions, such as the Arctic and northern China (Figs. 2c and 3c), likely due to climate feedbacks, remote teleconnection, and other processes. In general, the combined reductions of aerosols, ozone, and their precursors causes further warming, suggesting that the cooling effect of ozone reduction is significantly weaker than the warming effect of aerosol reduction.

3.2 Changes in temperature extremes in eastern and southern Asia

Figure 4 shows the time series of changes in annual mean extreme temperature indices averaged across the entire study area under the SSP3-7.0 and SSP3-7.0-lowNTCF scenarios from 2015 to 2050 relative to the reference period. All extreme temperature indices in the entire study area consistently increase under both scenarios, with a larger increase under the SSP3-7.0-lowNTCF scenario. By 2050, TXx and TX90p increase by 2.2 K and 27.7% under the SSP3-7.0 scenario and by 2.6 K and 34.9% under the SSP3-7.0-lowNTCF scenario, respectively. Compared to TXx and TX90, larger increases occur in TNn and TN90p, which increase by 2.8 K and 35.9% under the SSP3-7.0 scenario and 3.2 K and 43.1% under the SSP3-7.0-lowNTCF scenario, respectively. These changes indicate that future nighttime warming will be more apparent than daytime warming under both scenarios. Compared to the SSP3-7.0 scenario, non-methane SLCF emissions reductions cause additional warming of about 0.43 K for both TXx and TNn and increases of about 7.1% for both TX90p and TN90p. In addition, non-methane SLCF emissions reductions increases the TR and WSDI by 2.8 and 2.2 days by 2050, respectively.

Figure 5 shows the spatial patterns of changes in TXx, TX90p, TR, and WSDI over the entire study area during 2031–2050 relative to the reference period. Consistent increases occur in these extreme temperature indices under both the SSP3-7.0 and SSP3-7.0-lowNTCF scenarios. For TXx, In the SSP3-7.0 and SSP3-7.0-lowNTCF scenarios, the warming in most regions exceeds 1.5 K, and the warming is greater at higher latitudes under both scenarios, but the magnitude of the increase is larger under the SSP3-7.0-lowNTCF scenario than the SSP3-7.0 scenario. Such strong local effects of short-lived forcers to temperature extremes were also revealed in other high emission and population density regions (Sillmann et al., 2013a; Samset et al., 2018; Luo et al., 2020). The greatest changes in TXx, exceeding 5K, were simulated in RCP8.5 in such regions as South and North America, Eastern Europe, north-central Eurasia as well as Australia by the end of the 21st century (Sillmann et al., 2013a). Compared to the reference scenario, non-methane SLCF reduction leads to an additional increase of about 0.2 K across most of the entire study area's continent. Local effects of non-methane SLCF reductions are particularly large due to the short lifetimes of these contaminants. For example, future reductions in non-methane SLCFs cause TXx increases of more than 0.4 K in northern India and northern China, where anthropogenic emissions are high (Fig. 5c). For populated regions such as Europe, the United States and East Aisa, the TXx change in response to remove short-lived aerosol reductions is on average 25% stronger than global land-area mean (Samset et al., 2018).

Similarly, TX90p increases under both scenarios (Figs. 5d and e). In contrast to the changes in SAT (Fig. 2) and TXx, the increase in TX90p is more pronounced (>40%) at lower latitudes. This difference arises because high temperatures and lower daily temperature variation at low latitudes result in more days above the 90th percentile of the reference period. The largest increases in TX90p with non-methane SLCF reductions are found over India and eastern China, where increases are more than 8% and around 6%, respectively (Fig. 5f). In these regions, the effects of non-methane SLCFs are comparable to those of GHG forcing (Fig. 5d and f). TXx and TX90p indicate an increase in extreme daytime heat events, which not only increases the risk for heatstroke but also exacerbates ozone pollution, posing a further threat to human health (Gosling et al., 2009; Pu et al., 2017).

Concomitant with the increases in TNn and TN90p, TR is also projected to increase over the entire study area in the future. A significant increase of more than 40 days occurs in parts of southern India, the Indo-China Peninsula, and Indonesia, followed by eastern and northern China and Mongolia, with increases greater than 30 days, under the SSP3-7.0 scenario (Fig. 5g). The spatial pattern of TR changes under SSP3-7.0-lowNTCF is similar to that under SSP3-7.0, but the magnitude of the changes is larger (Fig. 5g and h). Non-methane SLCF reductions cause the largest increases in TR of more than 5 days in the Indo-China Peninsula, northern and northeastern China, and the Korean Peninsula (Fig. 5i). Notably, TR indicates that the temperature at night remains above 20 ℃. High nighttime temperatures can cause insomnia and abnormalities in thermoregulation, which may increase health risks, particularly for elderly or sick individuals (Fischer and Schär, 2010; Gosling et al., 2009).

With the increase in average temperature and values of extreme temperature indices described above, WSDI is also projected to increase significantly across the entire study area under both scenarios (Fig. 5j and k). Similar to TX90p, the increase in WSDI is more apparent at lower latitudes. The largest increments occur over the Qinghai-Tibet Plateau, southern China, and the Indo-China Peninsula. Compared to the SSP3-7.0 scenario, the increase in WSDI is greater under the SSP3-7.0-lowNTCF scenario, with increases of more than 12 days in the Qinghai-Tibetan Plateau, the Indo-China Peninsula, and along the coast of southern China. Non-methane SLCF reductions are associated with increases in WSDI of more than 2 days over almost the entire study area and more than 4 days in parts of northern China, coastal areas of southern China, northern India, and central and northern Asia (Fig. 5l).

Overall, the combined reductions of aerosols, ozone, and their precursors have an additional warming effect on Earth's climate system, exacerbating the surface warming and extreme temperature events caused by GHGs. These results are consistent with studies considering only aerosol reductions (Wang et al., 2016; Samset et al., 2018). Spatially, non-methane SLCF reductions cause the largest increases in extreme temperature indices in northern India and eastern China. In these regions, the human and environmental effects of temperature extremes are more significant due to high population densities and industrial development. Therefore, we selected northern India (NIN), northern China (NC), southern China (SC), and the Sichuan Basin (SCB) (Fig. 6a) for quantitative assessment of changes in regional mean extreme temperature indices in response to non-methane SLCF reductions.

The domain-averaged values of TXx, TX90p, TR, and WSDI across the entire study area have increases of 1.4 K, 37.4%, 8.9 days, and 9.1 days under the SSP3-7.0 scenario, respectively (Fig. 6). Considering the effects of non-methane SLCF reductions, these extreme temperature indices show increases of 1.7 K, 42.2%, 10.6 days, and 10.1 days under the SSP3-7.0-lowNTCF scenario, respectively. In general, the SCB is most strongly affected by extreme temperatures under both scenarios. Future reductions in non-methane SLCFs result in additional increases of 0.3 K in TXx, 4.8% in TX90p, 1.7 days in TR, and 1.0 days in WSDI for the entire study area. TXx, TX90p, and WSDI all show their largest regional increases in northern India and northern China, reaching 0.5 K, 8.5%, and 2.8 days and 0.4 K, 5.9%, and 3.0 days, respectively. The models agree on the sign of the change in TR across regions, and the largest increases occur in NC and the SCB, at 5.1 and 4.9 days, respectively. Although the MME changes in regional mean extreme temperature indices are consistently positive, some differences are found among the models, which may be attributed to differences in model resolution, the types of SLCFs included in each model, and parameterization schemes (Allen et al., 2020; Wei et al., 2019).

3.3 Changes in precipitation extremes in eastern and southern Asia

Figure 7 shows the time series of changes in annual mean precipitation indices averaged across the entire study area under the SSP3-7.0 and SSP3-7.0-lowNTCF scenarios from 2015 to 2050 relative to the reference period. Similar to the extreme temperature changes described above, the extreme precipitation changes are larger under the SSP3-7.0-lowNTCF scenario than the SSP3-7.0 scenario, and this difference increases gradually after 2030. By 2050, the values of R10, RX5day, and R95p have increased by 1.6 days, 2.7 days, and 46.7 mm under the SSP3-7.0 scenario, respectively. The increases in precipitation decrease drought events, resulting in a reduction in maximum CDD of 2.4 days. The non-methane SLCF reductions increase both R10 and RX5day by 1.0 day and R95p by 14.6 mm, but reduce CDD by 0.3 day (green dashed lines in Fig. 7).

Figure 8 shows the spatial patterns of extreme precipitation indices over the entire study area. Considering the spatial distribution of the changes in extreme precipitation indices, we selected NIN, NC, SC, and southwestern China (SWC) (Fig. 9a) for quantitative analysis of extreme precipitation changes. R10, RX5day, and R95p represent future changes in the intensity and frequency of extreme heavy precipitation. Under the SSP3-7.0 scenario, R10 decreases by approximately 2 days in central India, the Indo-China Peninsula, and by more than 4 days in the southeastern Qinghai-Tibet Plateau, SWC, and parts of Indonesia, while it increases in all other regions of the entire study area (Fig. 8a). Under the SSP3-7.0-lowNTCF scenario, R10 increases by 1.5 days across the entire study area, with the most significant increases of 1.9 days in SC and near the Himalayas. The reductions in non-methane SLCFs cause an increase of 1.0 days in average R10 across the entire study area. For the selected regions, the largest increases in R10 occur in SWC and SC, reaching .2.5 days and 1.5 days, respectively (Fig. 9b). In addition, significant increases of more than 3.0 days in R10 are found in the southeastern Qinghai-Tibet Plateau, India, the Indo-China Peninsula, and Indonesia; this pattern is exactly opposite of that of GHG forcing (Fig. 8a and c). By contrast, previous research suggested that reduction of aerosols alone will reduce R10 in these regions during 2031–2050 (Wang et al., 2016; Zhao et al., 2018).

RX5day increases across most of eastern and southern Asia under both future scenarios (Fig. 8d and e), with average increases of 1.7 mm and 2.7 mm under the SSP3-7.0 and SSP3-7.0-lowNTCF scenarios, respectively. The largest increases among the selected regions occur in SC, at 2.9 mm and 4.5 mm, respectively (Fig. 9c). Future reductions in non-methane SLCFs leads to an increase of 1.0 mm in RX5day in the entire study area. Regionally, these effects of non-methane SLCF reductions are much greater than the effects of GHG forcings alone. For example, non-methane SLCF mitigation yields an increase of 2.5 mm in RX5day in SWC, compared to 0.5 mm under the SSP3-7.0 scenario (Fig. 9c). In addition, non-methane SLCF reductions cause a significant increase of more than 2 mm in RX5day in the southeastern Qinghai-Tibet Plateau, the western Hengduan Mountains, SWC and the middle and lower reaches of the Yangtze River, whereas decreases of more than 3 mm occur in the southwestern part of the Indo-China Peninsula (Fig. 8f). The variation in RX5day can be used as an indicator of flooding and related hazards (Frich et al., 2002; Sillmann et al., 2013). Our results suggest that heavy precipitation associated with natural disasters will be aggravated in some parts of eastern and southern Asia in the future due to non-methane SLCF reductions.

The spatial pattern of changes in R95p is consistent with that of RX5day. With or without strong air quality controls, R95p increases across most of eastern and southern Asia, reaching 38.3 mm and 54.7 mm, respectively (Fig. 8g and h). The increases in R95p exceed 120 mm in the Himalayas, southeastern Qinghai-Tibet Plateau, western Hengduan Mountains, and Indonesia under the SSP3-7.0-lowNTCF scenario (Fig. 8h). Additional increases in R95p caused by reduced emissions of non-methane SLCFs are apparent in the southeastern Qinghai-Tibet Plateau, SWC and the middle and lower reaches of the Yangtze River (>40 mm), while significant decreases occur in the southwestern part of the Indo-China Peninsula (<-50 mm). R95p also decreases (<-10 mm) along the coast of SC (Fig. 8i), with effects greater than or comparable to GHGs in some regions. This finding is in opposition to previous results based on only aerosol reduction (Wang et al., 2016; Zhao et al., 2018).

In contrast to the three extreme precipitation indices described above, CDD represents the variability of extreme drought. In the entire study areat north of 30 °N, the increase in total precipitation reduces CDD, particularly at high latitudes. However, CDD increases in NIN, the southeastern Tibetan Plateau, and the southern Yangtze River (Fig. 8a and b). Overall, CDD decreases by 0.02 days and 0.4 days under the SSP3-7.0 and SSP3-7.0-lowNTCF scenarios, respectively. Future reductions in non-methane SLCFs contribute to significant decreases in CDD in northwestern and northeastern China, near the Hengduan Mountains, and the Indo-China Peninsula. CDD decreases by 1.0 days in SWC due to a significant increase in the frequency and intensity of heavy precipitation, and the sign of the results shows good agreement among models (Fig. 9e). Similarly, the changes in CDD due to non-methane SLCF reductions in some regions are comparable to the impacts of GHG forcing. Notably, the increases in CDD in India and eastern China are accompanied by increases in the frequency and intensity of extreme precipitation, which may be related to the probability distribution of future precipitation. A decrease in light rainfall and increase in heavy rainfall will lead to simultaneous increases in CDD and extreme precipitation (Wang et al., 2016). Zhu et al. (2021) showed that extreme precipitation in SC increases significantly while droughts become more severe under the SSP3-7.0 and SSP5-8.5 scenarios, suggesting that the future precipitation probability distribution function (PDF) distribution in SC could be more heterogeneous under high SSP scenarios.

In general, along with the increase in average temperature, future reductions in the emissions of non-methane SLCFs will increase the intensity and frequency of extreme precipitation and decrease the occurrence of extreme droughts in the entire study area. Previous studies have shown that the increase in aerosol emissions since the 1950s may have contributed to the anomalous precipitation pattern of “southern flood/northern drought” reported in eastern China and reduced precipitation in India (Bollasina et al., 2011; Li et al., 2016; Zhao et al., 2018), which will likely be mitigated by future aerosol reductions. Based on the spatial patterns of extreme precipitation indices described above, future combined reductions of aerosols, ozone, and their precursors will lead to marked increases of R10, RX5day, and R95p along with a decrease in CDD in northern China, which is consistent with the spatial pattern of precipitation when only aerosol emissions reduction is considered.

However, both extreme heavy precipitation and drought will increase in India. Consequently, our results indicate that future non-methane SLCF reductions may alleviate the observed precipitation anomaly pattern of “southern flood/northern drought” over eastern China, but may not have apparent mitigating effects on the precipitation reduction in India.

3.4 Population exposure to climate extremes in eastern and southern Asia

Extreme weather and climate events pose serious threats to human health, economic stability, and environmental sustainability, particularly in densely populated areas. Sustained warming of the climate will exacerbate climate extremes and the associated risks (Diffenbaugh et al., 2017; Sun et al., 2021). Based on the analysis presented above, reduction of non-methane SLCFs will further increase the frequency, intensity, and duration of extreme temperature and precipitation occurrences in eastern and southern Asia. Next, we analyze the changes in population exposure to extreme high temperature (TX90p) and heavy precipitation (R95p) under both future scenarios (Fig. 10).

Considering population growth and increased frequency of climate extremes, the total population exposed to TX90p and R95p show similar spatial patterns under the SSP3-7.0 and SSP3-7.0-lowNTCF scenarios, with the largest increases in India and eastern China (Fig. 10a, b, d, and e). Quantitatively, with the same population growth, a significantly greater population will be exposed to extreme temperature than to extreme heavy precipitation due to the higher frequency of extreme temperature events than extreme heavy precipitation events in the future. Under the SSP3-7.0 scenario, the largest increases in the population exposed to extreme temperature occur in India and eastern China, with a maximum increase greater than 6×10^8 person-days, while the increases in the population exposed to extreme precipitation exceed 4.5×10^7 person-days in India and are relatively small in eastern China (>1.5×10^7 person-days). Compared to the SSP3-7.0 scenario, future non-methane SLCF reduction will increase the population exposed to extreme temperature by more than 3.5×10^8 person-days in NIN, followed by 1.5×10^8 person-days in NC and the SCB. In addition, future non-methane SLCF reductions will significantly increase the population exposed to extreme precipitation in India, the SCB, and the middle and lower reaches of the Yangtze River, reaching values greater than 6×10^6 person-days.

Future changes in population exposure to climate extremes are affected by climate, population, and climate-population interactions according to equation (1) presented above. Under the SSP3 scenario, the population in India increases significantly by 2040 relative to 2000. This change is particularly sharp in NIN, which experiences an increase of more than 5 million people, followed by more than 1 million people in the SCB, NC and SC (data not shown). We attribute the changes in population exposure to three major factors (Figs. 11 and 12).

The increases in population exposed to extreme high temperatures are dominated by changes in climate factors under both the SSP3-7.0 and SSP3-7.0-lowNTCF scenarios in the four selected regions (Fig. 11). This result suggests that climate change caused by non-methane SLCF is the primary driver of population exposure to extreme temperature events, followed by changes in the climate-population interaction factor, with population change contributing the least. Future non-methane SLCF reductions increase population exposure to TX90p by $(32.2 \pm 11.4) \times 10^7$ person-days in NIN, $(10.3 \pm 5.2) \times 10^7$ person-days in NC, $(7.5 \pm 6.9) \times 10^7$ person-days in the SCB, and $(6.3 \pm 4.7) \times 10^7$ person-days in SC, respectively.

The climate factor is also the largest contributor to the increase in population exposure, followed by the climate-population interaction factor and the population factor in NC, the SCB, and SC (Fig. 12b-d). By contrast, the population factor becomes dominant in NIN, indicating that population growth is the main cause of increased population exposure in that region, followed by changes in the climate factor and climate-population interaction factor (Fig. 12a). Notably, in the SCB, greater changes in population exposure are caused by non-methane SLCF reductions than by the continued increase in GHGs (Fig. 12c). Future non-methane SLCF reductions increase total population exposure to R95p by (4.6. ± 6.1) $\times 10^6$ person-days in NIN, (2.0 ± 1.9) $\times 10^6$ person-days in NC, (3.6 ± 3.8) $\times 10^6$ person-days in the SCB, and (2.0 ± 2,2) $\times 10^6$ person-days in SC.

4 Discussion and conclusions

This study quantitatively assesses the impacts of reductions in emissions of non-methane SLCFs (including aerosols, ozone, and their precursors) on eastern and southern Asian climate extremes and the associated population exposure risks during 2031–2050 using MME simulations under the SSP3-7.0 and SSP3-7.0-lowNTCF scenarios from AerChemMIP. Our results show that non-methane SLCF reductions will exacerbate the warming effect caused by GHGs, resulting in increases in extreme temperature and precipitation events compared to the standard SSP3-7.0 scenario. These results are consistent with previous studies that have considered only aerosol reductions (Wang et al., 2016; Samset et al., 2018; Luo et al., 2020). Future reductions in non-methane SLCFs during 2031–2050 are projected to cause a global mean ERF of 0.23 ± 0.16 W m^{-2} and an increase of 0.19 ± 0.1 K in global average SAT relative to 1995–2014 based on the MME results.

The additional warming caused by the reduction of non-methane SLCF emissions increases domain-averaged TXx by 0.3 ± 0.1 K, TX90p by 4.8 ± 2.2 %, TR by 1.7 ± 0.8 days, and WSDI by 1.0 ± 0.4 days across the entire study area. Regionally, TXx, TX90p, and WSDI show their largest increases in NIN and NC, reaching 0.5 ± 0.2 K, 8.5 ± 2.9 %, and 2.8 ± 1.1 days and 0.4 ± 0.2 K, 5.9 ± 2.7%, and 3.0 ± 1.3 days, respectively. The increase in TX90p due to non-methane SLCF mitigation is comparable to that caused by GHG emissions in some regions. The models agree on the sign of the change in TR across regions, with the largest increases in NC and the SCB reaching 5.1 ± 2.5 and 4.9 ± 3.3 days, respectively. Overall, the warming trends driven by the combined reductions of aerosols, ozone, and their precursors are similar to the trends driven only by aerosol reductions. In addition, population exposure to TX90p associated with future non-methane SLCF reductions is greatest in NIN, at (32.2 ± 11.4) $\times 10^7$ person-days.

For extreme precipitation, future non-methane SLCF reductions increase domain-averaged R10 by 1.0 ± 0.5 days, RX5day by 1.0 ± 0.32 mm, and R95p by 16.4 ± 7.3 mm in the entire study area. In SWC, R10, RX5day, and R95p increase by 2.5 ± 1.9 days, 2.5 ± 1.5 mm, and 37.5 ± 22.6 mm, and these increases are greater or comparable to the effects of GHGs. By contrast, CDD decreases by 1.4 days in SWC due to significant increases in the frequency and intensity of heavy precipitation events. Notably, large differences in extreme precipitation changes are found at the regional scale in response to reductions of non-methane SLCFs and only aerosols, with changes in opposite directions observed in some regions. This discrepancy may be attributed to ozone and aerosol interactions, which may be further assessed via model simulations with both coupled and uncoupled experiments in the future. The spatial pattern of changes in the total population exposed to R95p due to non-methane SLCF reductions is largely consistent with the distribution of TX90p, with the largest increases in NIN reaching $(4.6 \pm 6.1) \times 10^6$ person-days.

Compared with previous assessment by Allen et al. (2020), our study provides some new insights for the effects of future non-methane SLCF emissions on regional climate change. Firstly, although extreme temperature indices are all increasing in the future due to the reduction of non-methane SLCFs, TX90p and WSDI vary spatially opposite to TXx, indicating that the warming of future temperature extremes is greater at higher latitudes, while the increase in the frequency and duration of extreme temperature occurrences is more pronounced at lower latitudes. As for extreme precipitation, changes in both R10 and R95p in some areas are contrary to previous results considering only aerosol reduction, revealing the importance of considering aerosol and ozone interactions. More importantly, we analyze the changes in TR and RX5day. The former represents the variation of nighttime temperature extremes that are important for human health. The latter is usually used as an indicator of flooding, suggesting that heavy precipitation associated with natural disasters will be aggravated in the future due to non-methane SLCFs reduction. Secondly, population exposure can provide a well assessment of future climate change risk. The reduction of non-methane SLCFs will result in the exposure of millions of people to extreme events, and up to tens of millions in densely populated areas, such as northern India, which is an indicator of human health risk and also valuable for future policy making on climate change mitigation and adaptation, Thirdly, Allen et al. (2020) used nine models, including five Aer+O_3 models and four Aer-only models, but we used seven Aer+O_3 models. The more Aer+O_3 models may better reflect the effect of considering the combined aerosol and ozone changes simultaneously. Finally, Pendergrass et al. (2019) have shown that the response of extreme precipitation to warming varies widely in climate models, especially in the tropics. The rate of response increases with warming is not linear but non-linear (Pendergrass et al., 2019), as shown in Allen et al. (2020) that some of the extreme indices were not well fitted. Freychet et al. (2019) suggested that radiation-driven aerosol emission impacts on local surface temperature and precipitation were not linear and could be mitigated or cancelled by the local dynamics. Our method of subtracting the mean between two periods may, to some extent, provide a more intuitive representation of the changes in the extreme indices in absolute terms.

Notably, GHGs share many common sources with SLCFs, such as the combustion of fossil fuels. Emission reductions for shorter-lived GHGs, such as methane, can partially mask or offset the warming caused by emission reductions of non-methane SLCFs over decades, providing benefits for both climate change mitigation and air quality on nearly all decadal to centennial time scales (Allen et al., 2021; Shindell and Smith, 2019). Increasing and accumulating anthropogenic GHG emissions are the main driving factor in shaping the increase and intensification of extreme high temperatures globally and regionally. By the end of the century, the differences in temperature and precipitation between the different aerosol reduction scenarios are negligible in the context of ambitious CO2 reductions (Hienola et al., 2018; Wilcox et al., 2020), and global warming is significantly less under strong mitigation scenarios with both climate policies and air quality controls (i.e., SSP1-1.9 and SSP1-2.6) than under the SSP3-7.0-lowNTCF scenario with only strong air quality control measures (Naik et a., 2021). Even if the impact of non-methane SLCFs is negligible on centennial time scales, they may be important for regional and global climate in the coming decade, especially for Asia where aerosol has played an important role in historical changes, in particular for precipitation (Wilcox et al., 2020). The important impact of SLCFs on climate change in the short term does not mean that reducing air pollutants is harmful to the climate, but rather that it generates additional warming to the climate, amplifying the temperature and extreme precipitation caused by GHGs changes (Wang et al., 2016; Luo et al., 2020). In the short term, the differences in regional climate change under different future emission scenarios depend strongly on changes in emissions of SLCFs, especially before net CO_2 emissions (and co-emitted aerosol emissions) become very low in the first half of this century (Hienola et al., 2018; Wilcox et al., 2020). Warming is most obvious in the strong mitigation scenarios (i.e., SSP1-1.9 and SSP1-2.6) because of the rapid reduction in aerosols. In the SSP3-7.0 scenario, aerosols do not decrease until mid-century, but increases in methane and ozone contribute to the net warming in 2040. The warming is similar in magnitude to the SSP1 scenario, where aerosol reductions are the primary driver (Wilcox et al. 2020; Naik et al. 2021). Also, the conclusion of Shindell and Smith (2019) that there is no conflict between climate and air quality objectives may not hold when using a full coupled global climate model and when investigating changes beyond global mean temperature (Wilcox et al., 2020). Although it is difficult to improve air quality alone without reducing GHGs in reality, this is the case for some air quality policies, such as flue gas desulfurization in coal-fired power plants, denitrification, restaurant grease pollution control, and improved vehicle emission standards. These advanced end-of-pipe control measures may involve only the reduction of air pollutants (Rafaj et al., 2014; Hordijk and Amann, 2007). For example, European countries have taken specific measures to reduce air pollutant emissions, especially through the application of advanced end-of-pipe emission control technologies, resulting in a significant decline in SO_2 and NOx emissions in Western Europe after the 1970s, compared to a constant growth rate of CO_2 emissions (Rafaj et al., 2014; Hordijk and Amann, 2007). For China, the State Council implemented the Air Pollution Prevention and Control Action Plan in 2013 and the Three-Year Action Plan to Win the Blue Sky Defense War implemented in 2018 both introduced a series of aggressive industrial clean air policies (Zheng et al., 2018; Cheng et al., 2019). The reality in China's air pollution prevention and control policies in recent years is that China's treatment is still dominated by end-of-pipe measures, as source treatment often requires large investments to ensure energy efficiency and is not conducive to maintaining the competitiveness of Chinese industry (Wu et al., 2019), in which case it may only result in rapid reductions in air pollutants. Besides, emissions reductions aimed at achieving global carbon neutrality will inevitably result in further reductions in SLCF emissions, as demonstrated in the SSP1-1.9 and SSP1-2.6 scenarios (Gidden et al., 2019), which may lead to greater impacts of SLCFs on climate. The maximum technical potential in SSP3-7.0-lowNTCF scenario refers to the currently existing end-of-pipe technologies, with faster technological progress and stronger air quality action, greater emission reductions may also be possible, which may cause greater impacts on climate. Additionally, cleaner air may already has increased the warming effect of CO_2 emissions over the past two decades, and this will get worse as air pollution continues to be controlled (Quaas et al., 2022; McKenna et al., 2021). Finally, large biases may exist in SLCF emissions at the regional scale in global emissions scenarios due to insufficient consideration of local environmental policies (Tong et al., 2020). For example, the SSP-RCP global emissions scenarios used in CMIP6 do not fully consider the rapid pollution controls enacted in China since 2013 under the Air Pollution Prevention and Control Action Plan. Consequently, the emissions trends in the SSP scenarios after 2014 differ significantly from actual conditions in China (Wang et al., 2021; Tong et al., 2020), which may lead to underestimation of the impact of SLCF emissions reductions in China. This study highlights the importance of reductions in emissions of non-methane SLCFs for future climate change and population exposure risk in eastern and southern Asia in the short term and suggests that current and future policy decisions about air pollution emissions have the potential for a large near-term impact on temperature and precipitation extremes. What policymakers, the public or the media need to know is that air pollution is dangerous to human health, and there is no doubt that we need clean air, but more importantly efforts to reduce GHGs need to be doubled in order to simultaneously mitigate climate change and improve air quality (Quaas et al., 2022; McKenna et al., 2021).

Data availability. The CMIP6 Historical and AerChemMIP model data can be freely downloaded from https://esgf-node.llnl.gov/projects/cmip6. The observed gridded data can be downloaded at the website of https://psl.noaa.gov/data/gridded/index.html. Gridded population datasets for the base year and future under SSP3 scenario are publicly available at https://www.cgd. ucar.edu/iam/modeling/spatial-population-scenarios.

Author contributions. ZW conceived the study. YL performed the analysis. YL, ZW, and YL led the paper writing. All authors provided comments and contributed to the text.

Competing interests. The authors declare that they have no conflict of interest.

Acknowledgments. This study was supported by the National Natural Science Foundation of China (42275042 and 41875179) and the Science and technology development fund of CAMS (2022KJ004).

References

Allen, J. R., Turnock, S., Nabat, P., Neubauer, D., Lohmann, U., Olivié, D., Oshima, N., Michou, M., Wu, T., Zhang, J., Takemura, T., Schulz, M., Tsigaridis, K., E. Bauer, S., Emmons, L., Horowitz, L., Naik, V., Van Noije, T., Bergman, T., Lamarque, J. F., Zanis, P., Tegen, I., M. Westervelt, D., Le Sager, P., Good, P., Shim, S., O'Connor, F., Akritidis, D., Georgoulias, A. K., Deushi, M., T. Sentman, L., G. John, J., Fujimori, S., and J. Collins, W.: Climate and air quality impacts due to mitigation of non-methane near-term climate forcers, Atmos. Chem. Phys., 20, 9641–9663, https://doi.org/10.5194/acp-20-9641-2020, 2020.

Allen, J.R., Horowitz, W. L., Naik, V., Oshima, N., O'Connor, M. F., Turnock, S., Shim, S., Sager, L. P., Noije, V. T., Tsigaridis, K., Bauer, E. S., Sentman, L. T., John, J. G., Broderick, C., Deushi, M., Folberth, A. G., Fujimori, S., and Collins, J.W.: Significant climate benefits from near-term climate forcer mitigation in spite of aerosol reductions, Environ. Res. Lett. 16, 034010, https://doi.org/10.1088/1748-9326/abe06b, 2021.

An, J., Fu, B., Li W., Peng, S., Li, B.: Future Prediction of Typical Extreme Climatic Indices and Population Exposure to High Temperature in East Asia. Acta Scientiarum Naturalium Universitatis Pekinensis, 56, 884–892, https://doi.org/10.13209/j.0479-8023.2020.071, 2020.

Apte, J. S., Marshall, J. D., Cohen, A. J., and Brauer, M.: Addressing Global Mortality from Ambient PM2.5., Environ. Sci. Technol., 49, 8057–8066, https://doi.org/10.1021/acs.est.5b01236, 2015.

Baker, L., Collins, W., Olivié, D., Cherian, R., Hodnebrog, Ø., Myhre, G., and Quaas, J.: Climate responses to anthropogenic emissions of short-lived climate pollutants, Atmos. Chem. Phys., 15, https://doi.org/10.5194/acp-15-8201-2015, 2015.

Bollasina, M. A., Yi, M., and V., R.: Anthropogenic Aerosols and the Weakening of the South Asian Summer Monsoon, Science, 334, 502–505, https://doi.org/10.1126/science.1204994, 2011.

Bras, T.A., Seixas, J., Carvalhais, N., Jagermeyr, J., 2021. Severity of drought and heatwave crop losses tripled over the last five decades in Europe. Environ. Res. Lett. 16 (6), 065012 https://doi.org/10.1088/1748-9326/abf004.

Chang, W., Liao, H., and Wang, H.: Climate responses to direct radiative forcing of anthropogenic aerosols, tropospheric ozone, and long-lived greenhouse gases in eastern China over 1951–2000, Adv. Atmos. Sci., 26, 748–762, https://doi.org/10.1007/s00376-009-9032-4, 2009.

Chen, H. and Sun, J.: Increased population exposure to extreme droughts in China due to 0.5 ℃ of additional warming, Environ. Res. Lett., 14, https://doi.org/10.1088/1748-9326/ab072e, 2019.

Chen, H. and Sun, J.: Increased population exposure to precipitation extremes in China under global warming scenarios, Atmos. Ocean. Sci. Lett., 13, 63–70, https://doi.org/10.1080/16742834.2020.1697168, 2020.

Chen, H., Sun, J., and Li, H.: Increased population exposure to precipitation extremes under future warmer climates, Environ. Res. Lett., 15, https://doi.org/10.1088/1748-9326/ab751f, 2020.

Chen, H., Sun, J., Lin, W., and Xu, H.: Comparison of CMIP6 and CMIP5 models in simulating climate extremes, Sci. Bull., 65, 1415-1418, https://doi.org/10.1016/j.scib.2020.05.015, 2020a.

Chen, H., Sun, J., and Li, H.: Increased population exposure to precipitation extremes under future warmer climates, Environ. Res. Lett., 15, https://doi.org/10.1088/1748-9326/ab751f, 2020b.

Chen, J., Liu, Y., Pan, T., Liu, Y., Sun, F., and Ge, Q.: Population exposure to droughts in China under the 1.5℃ global warming target, Earth Syst. Dyn., 9, 1097–1106, https://doi.org/10.5194/esd-9-1097-2018, 2018.

Chuwah, C., van Noije, T., van Vuuren, D. P., Le Sager, P., and Hazeleger, W.: Global and regional climate impacts of future aerosol mitigation in an RCP6.0-like scenario in EC-Earth, Clim. Change, 134, 1–14, https://doi.org/10.1007/s10584-015-1525-9, 2016.

Collins, J. W., Lamarque, J. F., Schulz, M., Boucher, O., Eyring, V., Hegglin, I. M., Maycock, A., Myhre, G., Prather, M., Shindell, D., and Smith, J. S.: AerChemMIP: Quantifying the effects of chemistry and aerosols in CMIP6, Geosci. Model Dev., 10, 585–607, https://doi.org/10.5194/gmd-10-585-2017, 2017.

Diffenbaugh N. S., Singh, D., Mankin. J. S., Horton, D.E., H. D., Swain, D.L., Touma, D,. Charland, A., Liu, Y., Haugen, M., Tsang, M., and Rajaratnam, B.: Quantifying the influence of global warming on unprecedented extreme climate events, Proc. Natl. Acad. Sci., 114, 4881–4886, https://doi.org/10.1073/pnas.1618082114, 2017.

Dong, B., Wilcox, L. J., Highwood, E. J., and Sutton, R. T.: Impacts of recent decadal changes in Asian aerosols on the East Asian summer monsoon: roles of aerosol–radiation and aerosol–cloud interactions, Clim. Dyn., 53, 3235–3256, https://doi.org/10.1007/s00382-019-04698-0, 2019.

Fan, X., Miao, C., Duan, Q., Shen, C., and Wu, Y.: The Performance of CMIP6 Versus CMIP5 in Simulating Temperature Extremes Over the Global Land Surface, J. Geophys. Res. Atmos., 125, 1-16, https://doi.org/10.1029/2020JD033031, 2020.

Fischer, E. M. and Schär, C.: Consistent geographical patterns of changes in high-impact European heatwaves, Nat. Geosci., 3, 398–403, https://doi.org/10.1038/ngeo866, 2010.

Forster, P. M., Richardson, T., Maycock, A. C., Smith, C. J., Samset, B. H., Myhre, G., Andrews, T., Pincus, R., and Schulz, M.: Recommendations for diagnosing effective radiative forcing from climate models for CMIP6, J. Geophys. Res. Atmos., 121, 12,412-460,475, https://doi.org/https://doi.org/10.1002/2016JD025320, 2016.

Freychet, N., Tett, S. F. B., Bollasina, M., Wang, K. C., and Hegerl, G. C.: The Local Aerosol Emission Effect on Surface Shortwave Radiation and Temperatures, J. Adv. Model. Earth Syst., 11, 806-817, https://doi.org/https://doi.org/10.1029/2018MS001530, 2019.

Frich, P.L., Alexander, L., Della-Marta, P., Gleason, B., Haylock, M., Klein, T., and Peterson, T.C.: Observed coherent changes in climatic extremes during 2nd half of the 20th century, Clim. Res., 19, https://doi.org/10.3354/cr019193, 2002.

Fujimori, S., Hasegawa, T., Masui, T., Takahashi, K., Herran, D. S., Dai, H., Hijioka, Y., and Kainuma, M.: SSP3: AIM implementation of Shared Socioeconomic Pathways, Glob. Environ. Chang., 42, 268-283, https://doi.org/https://doi.org/10.1016/j.gloenvcha.2016.06.009, 2017.

Gidden, M. J., Riahi, K., Smith, S. J., Fujimori, S., Luderer, G., Kriegler, E., van Vuuren, D. P., van den Berg, M., Feng, L., Klein, D., Calvin, K., Doelman, J. C., Frank, S., Fricko, O., Harmsen, M., Hasegawa, T., Havlik, P., Hilaire, J., Hoesly, R., Horing, J., Popp, A., Stehfest, E., and Takahashi, K.: Global emissions pathways under different socioeconomic scenarios for use in CMIP6: a dataset of harmonized emissions trajectories through the end of the century, Geosci. Model Dev., 12, 1443–1475, https://doi.org/10.5194/gmd-12-1443-2019, 2019.

Gosling, S. N., Lowe, J. A., McGregor, G. R., Pelling, M., and Malamud, B. D.: Associations between elevated atmospheric temperature and human mortality: a critical review of the literature, Clim. Change, 92, 299–341, https://doi.org/10.1007/s10584-008-9441-x, 2009.

Guo, D., Zhang, Y., Gao, X., Pepin, N., and Sun, J.: Evaluation and ensemble projection of extreme high and low temperature events in China from four dynamical downscaling simulations, Int. J. Climatol., 41, E1252–E1269, https://doi.org/10.1002/joc.6765, 2021.

Hienola, A., Partanen, A. I., Pietikäinen, J. P., O'Donnell, D., Korhonen, H., Matthews, H. D., and Laaksonen, A.: The impact of aerosol emissions on the 1.5 °C pathways, Environ. Res. Lett., 13, 44011, https://doi.org/10.1088/1748-9326/aab1b2, 2018.

Hoesly, R. M., Smith, S. J., Feng, L., Klimont, Z., Janssens-Maenhout, G., Pitkanen, T., Seibert, J. J., Vu, L., Andres, R. J., Bolt, R. M., Bond, T. C., Dawidowski, L., Kholod, N., Kurokawa, J.-I., Li, M., Liu, L., Lu, Z., Moura, M. C. P., O'Rourke, P. R., and Zhang, Q.: Historical (1750–2014) anthropogenic emissions of reactive gases and aerosols from the Community Emissions Data System (CEDS), Geosci. Model Dev., 11, 369–408, https://doi.org/10.5194/gmd-11-369-2018, 2018.

Hordijk, L. and Amann, M.: How science and policy combined to combat air pollution problems, Environ. Policy Law, 37, 336-340, 2007.

Jenkins, S., Povey, A., Gettelman, A., Grainger, R., Stier, P., and Allen, M.: Is Anthropogenic Global Warming Accelerating?, J. Clim., 1-43, https://doi.org/10.1175/jcli-d-22-0081.1, 2022.

Jones, B. and O'Neill, B. C.: Spatially explicit global population scenarios consistent with the Shared Socioeconomic Pathways, Environ. Res. Lett., 11, https://doi.org/10.1088/1748-9326/11/8/084003, 2016.

Jones, B., O'Neill, B. C., McDaniel, L., McGinnis, S., Mearns, L. O., and Tebaldi, C.: Future population exposure to US heat extremes, Nat. Clim. Chang., 5, 652–655, https://doi.org/10.1038/nclimate2631, 2015.

Kim, Y. H., Min, S. K., Zhang, X., Sillmann, J., and Sandstad, M.: Evaluation of the CMIP6 multi-model ensemble for climate extreme indices, Weather Clim. Extrem., 29, 100269, https://doi.org/10.1016/j.wace.2020.100269, 2020.

King, A. D., Knutti, R., Uhe, P., Mitchell, D. M., Lewis, S. C., Arblaster, J. M., and Freychet, N.: On the Linearity of Local and Regional Temperature Changes from 1.5 ℃ to 2 ℃ of Global Warming, J. Clim., 31, 7495–7514, https://doi.org/10.1175/JCLI-D-17-0649.1, 2018.

Li, S., Wang, T., Zanis, P., Melas, D., and Zhuang, B.: Impact of Tropospheric Ozone on Summer Climate in China, J. Meteorol. Res., 32, 279–287, https://doi.org/10.1007/s13351-018-7094-x, 2018.

Li, Z., Lau, W., Ramanathan, V., Wu, G., Ding, Y., Manoj, M. G., Liu, J., Qian, Y., Li, J., Zhou, T., Fan, J., Rosenfeld, D., Ming, Y., Wang, Y., Huang, J., Wang, B., Xu, X., Lee, S.-S., Cribb, M., and Zhao, C.: Aerosol and Monsoon Climate Interactions over Asia: Aerosol and Monsoon Climate Interactions, Rev. Geophys., 54, https://doi.org/10.1002/2015RG000500, 2016.

Liao, H., Chang, W., and Yang, Y.: Climatic effects of air pollutants over china: A review, Adv. Atmos. Sci., 32, 115–139, https://doi.org/10.1007/s00376-014-0013-x, 2015.

Lin, L., Wang, Z., Xu, Y., and Fu, Q.: Sensitivity of precipitation extremes to radiative forcing of greenhouse gases and aerosols, Geophys. Res. Lett., 43, 9860–9868, https://doi.org/10.1002/2016GL070869, 2016.

Lin, L., Xu, Y., Wang, Z., Diao, C., Dong, W., and Xie, S.-P.: Changes in Extreme Rainfall Over India and China Attributed to Regional Aerosol-Cloud Interaction During the Late 20th Century Rapid Industrialization, Geophys. Res. Lett., 45, 7857–7865, https://doi.org/https://doi.org/10.1029/2018GL078308, 2018.

Luo, F., Wilcox, L., Dong, B., Su, Q., Chen, W., Dunstone, N., Li, S., and Gao, Y.: Projected near-term changes of temperature extremes in Europe and China under different aerosol emissions, Environ. Res. Lett., 15, 34013, https://doi.org/10.1088/1748-9326/ab6b34, 2020.

Malley, C. S., Henze, D. K., Kuylenstierna, J. C. I., Vallack, H. W., Davila, Y., Anenberg, S. C., Turner, M. C., and Ashmore, M. R.: Updated Global Estimates of Respiratory Mortality in Adults ≥30Years of Age Attributable to Long-Term Ozone Exposure., Environ. Health Perspect., 125, 87021, https://doi.org/10.1289/EHP1390, 2017.

McKenna, C. M., Maycock, A. C., Forster, P. M., Smith, C. J., and Tokarska, K. B.: Stringent mitigation substantially reduces risk of unprecedented near-term warming rates, Nat. Clim. Change., 11, 126-131, https://doi.org/10.1038/s41558-020-00957-9, 2021.

Mirza, M.: Climate change, flooding in South Asia and implications . Reg. Environ. Change, 11. https://doi.org/10.1007/s10113-010-0184-7. 2011.

Mu, J. and Wang, Z.: Responses of the East Asian summer monsoon to aerosol forcing in CMIP5 models: The role of upper-tropospheric temperature change, Int. J. Climatol., 41, 1555–1570, https://doi.org/10.1002/joc.6887, 2021.

Myhre, G., Shindell, D., Bréon, F.-M., Collins, W., Fuglestvedt, J., Huang, J., Koch, D., Lamarque, J.-F., Lee, D., Mendoza, B., Nakajima, T., Robock, A., Stephens, G., Takemura, T., and Zhang, H.: Anthropogenic and Natural Radiative Forcing, in Climate Change 2013: The Physical Science Basis. Contribution of Working Group I to the Fifth Assessment Report of the Intergovernmental Panel on Climate Change, Stocker, T. F., Qin, D., Plattner, G.-K., Tignor, M., Allen, S. K., Boschung, J., Nauels, A., Xia, Y., Bex, V., and Midgley, P. M. (Eds.), Tech. rep., Cam- bridge University Press, Cambridge, United Kingdom and New York, NY, USA, 2013.

Naik, V., Szopa, S., Adhikary, B., Artaxo, P., Berntsen, T., Collins, W. D., Fuzzi, S., Gallardo, L., Kiendler Scharr, A., Klimont, Z., Liao, H., Unger, N., and Zanis, P.: Short-Lived Climate Forcers. In: Climate Change 2021: The Physical Science Basis. Contribution of Working Group I to the Sixth Assessment Report of the Intergovernmental Panel on Climate Change, Masson-Delmotte, V., Zhai, P., Pirani, A., Connors, S. L., Péan, C., Berger, S., Caud, N., Chen, Y., Goldfarb, L., Gomis, M. I., Huang, M., Leitzell, K., Lonnoy, E., Matthews, J. B. R., Maycock, T. K., Waterfield, T., Yelekçi, O., Yu R. and Zhou B. (Eds.), Cambridge University Press. In Press. 2021.

Patz, J. A., Campbell-Lendrum, D., Holloway, T., and Foley, J. A.: Impact of regional climate change on human health, Nature, 438, 310-317, https://doi.org/10.1038/nature04188, 2005.

Pendergrass, A. G., Coleman, D. B., Deser, C., Lehner, F., Rosenbloom, N., and Simpson, I. R.: Nonlinear Response of Extreme Precipitation to Warming in CESM1, Geophys. Res. Lett., 46, 10551-10560, https://doi.org/https://doi.org/10.1029/2019GL084826, 2019.

Piao, S., Ciais, P., Huang, Y., Shen, Z., Peng, S., Li, J., Zhou, L., Liu, H., Ma, Y., Ding, Y., Friedlingstein, P., Liu, C., Tan, K., Yu, Y., Zhang, T., and Fang, J.: The impacts of climate change on water resources and agriculture in China, Nature, 467, 43-51, https://doi.org/10.1038/nature09364, 2010.

Pincus, R., Forster, P., and Stevens, B.: The Radiative Forcing Model Intercomparison Project (RFMIP): Experimental Protocol for CMIP6, Geosci. Model Dev. Discuss., 1–18, https://doi.org/10.5194/gmd-2016-88, 2016.

Pu, X., Wang, T. J., Huang, X., Melas, D., Zanis, P., Papanastasiou, D. K., and Poupkou, A.: Enhanced surface ozone during the heat wave of 2013 in Yangtze River Delta region, China, Sci. Total Environ., 603–604, 807–816, https://doi.org/https://doi.org/10.1016/j.scitotenv.2017.03.056, 2017.

Quaas, J., Jia, H., Smith, C., Albright, A. L., Aas, W., Bellouin, N., Boucher, O., Doutriaux-Boucher, M., Forster, P. M., Grosvenor, D., Jenkins, S., Klimont, Z., Loeb, N. G., Ma, X., Naik, V., Paulot, F., Stier, P., Wild, M., Myhre, G., and Schulz, M.: Robust evidence for reversal in the aerosol effective climate forcing trend, Atmos. Chem. Phys. Discuss., 2022, 1-25, 2022.

Rafaj, P., Amann, M., Siri, J., and Wuester, H.: Changes in European greenhouse gas and air pollutant emissions 1960-2010: Decomposition of determining factors, Clim. Change, 124, 477-504, https://doi.org/10.1007/s10584-013-0826-0, 2014.

Ramanathan, V., Li, F., Ramana, M. V, Praveen, P. S., Kim, D., Corrigan, C. E., Nguyen, H., Stone, E. A., Schauer, J. J., Carmichael, G. R., Adhikary, B., and Yoon, S. C.: Atmospheric brown clouds: Hemispherical and regional variations in long-range transport, absorption, and radiative forcing, J. Geophys. Res. Atmos., 112, https://doi.org/https://doi.org/10.1029/2006JD008124, 2007.

Samset, B. H., Sand, M., Smith, C. J., Bauer, S. E., Forster, P. M., Fuglestvedt, J. S., Osprey, S., and Schleussner, C. F.: Climate Impacts From a Removal of Anthropogenic Aerosol Emissions, Geophys. Res. Lett., 45, 1020–1029, https://doi.org/10.1002/2017GL076079, 2018.

Shindell, D. and Smith, C. J.: Climate and air-quality benefits of a realistic phase-out of fossil fuels, Nature, 573, 408-411, https://doi.org/10.1038/s41586-019-1554-z, 2019.

Sillmann, J., Kharin, V. V, Zwiers, F. W., Zhang, X., and Bronaugh, D.: Climate extremes indices in the CMIP5 multi-model ensemble: Part 2. Future climate projections, J. Geophys. Res. Atmos., 118, 2473–2493, https://doi.org/https://doi.org/10.1002/jgrd.50188, 2013a.

Sillmann, J., Kharin, V. V., Zhang, X., Zwiers, F. W., and Bronaugh, D.: Climate extremes indices in the CMIP5 multimodel ensemble: Part 1. Model evaluation in the present climate, J. Geophys. Res. Atmos., 118, 1716-1733, https://doi.org/10.1002/jgrd.50203, 2013b.

Smith, C. J., Forster, P. M., Allen, M., Leach, N., Millar, R. J., Passerello, G. A., and Regayre, L. A.: FAIR v1.3: a simple emissions-based impulse response and carbon cycle model, Geoscientific Model Development, 11,2297, https://doi.org/10.5194/gmd-11-2273-2018, 2018.

Sun, S., Dai, T. L., Wang, Z. Y., Chou, J. M., Chao, Q. C., and Shi, P. J.: Projected increases in population exposure of daily climate extremes in eastern China by 2050, Adv. Clim. Chang. Res., https://doi.org/10.1016/j.accre.2021.09.014, 2021.

Sun, X., Ge, F., Fan, Y., Zhu, S., and Chen, Q.: Will population exposure to heat extremes intensify over Southeast Asia in a warmer world?, Environ. Res. Lett., 17, 44006, https://doi.org/10.1088/1748-9326/ac48b6, 2022.

Tellman, B., Sullivan, J. A., Kuhn, C., Kettner, A. J., Doyle, C. S., Brakenridge, G. R., Erickson, T. A., and Slayback, D. A.: Satellite imaging reveals increased proportion of population exposed to floods, Nature, 596, 80–86, https://doi.org/10.1038/s41586-021-03695-w, 2021.

Tong, D., Cheng, J., Liu, Y., Yu, S., Yan, L., Hong, C., Qin, Y., Zhao, H., Zheng, Y., Geng, G., Li, M., Liu, F., Zhang, Y., Zheng, B., Clarke, L., and Zhang, Q.: Dynamic projection of anthropogenic emissions in China: methodology and 2015--2050 emission pathways under a range of socio-economic, climate policy, and pollution control scenarios, Atmos. Chem. Phys., 20, 5729–5757, https://doi.org/10.5194/acp-20-5729-2020, 2020.

Turnock, S., Allen, R., Andrews, M., Bauer, S., Emmons, L., Good, P., Horowitz, L., Michou, M., Nabat, P., Naik, V., Neubauer, D., O'Connor, F., Olivié, D., Schulz, M., Sellar, A., Takemura, T., Tilmes, S., Tsigaridis, K., Wu, T., and Zhang, J.: Historical and future changes in air pollutants from CMIP6 models, Atmos. Chem. Phys., 1-40, https://doi.org/10.5194/acp-2019-1211, 2020.

Wang, Z., Lin, L., Xu, Y., Che, H., Zhang, X., Zhang, H., Dong, W., Wang, C., Gui, K., and Xie, B.: Incorrect Asian aerosols affecting the attribution and projection of regional climate change in CMIP6 models, npj Clim. Atmos. Sci., 4, 2, https://doi.org/10.1038/s41612-020-00159-2, 2021.

Wang, Z., Lin, L., Yang, M., and Guo, Z.: The Role of Anthropogenic Aerosol Forcing in Interdecadal Variations of Summertime Upper-Tropospheric Temperature Over East Asia, Earth's Futur., 7, 136–150, https://doi.org/10.1029/2018EF001052, 2019.

Wang, Z., Lin, L., Yang, M., and Xu, Y.: The effect of future reduction in aerosol emissions on climate extremes in China, Clim. Dyn., 47, 2885–2899, https://doi.org/10.1007/s00382-016-3003-0, 2016.

Wang, Z., Mu, J., Yang, M., and Yu, X.: Reexamining the mechanisms of East Asian summer monsoon changes in response to non-East Asian anthropogenic aerosol forcing, J. Clim., 33, 2929–2944, https://doi.org/10.1175/JCLI-D-19-0550.1, 2020.

Wei, Y., Chen, X., Chen, H., Li, J., Wang, Z., Yang, W., Ge, B., Du, H., Hao, J., Wang, W., Li, J., Sun, Y., and Huang, H.: IAP-AACM v1.0: a global to regional evaluation of the atmospheric chemistry model in CAS-ESM, Atmos. Chem. Phys., 19, 8269–8296, https://doi.org/10.5194/acp-19-8269-2019, 2019.

Weisskopf, M. G., Anderson, H. A., Foldy, S.L., Hanrahan, P., Blair, K. T., Trk, J., and Rumm, P. D.: Heat wave morbidity and mortality,Milwaukee, Wis, 1999 vs 1995: An improved response?,Am. J. PublicHealth,92, 830-833, 2002.

Westervelt, D. M., Conley, A. J., Fiore, A. M., Lamarque, J. F., Shindell, D. T., Previdi, M., Mascioli, N. R., Faluvegi, G., Correa, G., and Horowitz, L. W.: Connecting regional aerosol emissions reductions to local and remote precipitation responses, Atmos. Chem. Phys., 18, 12461–12475, https://doi.org/10.5194/acp-18-12461-2018, 2018.

Westervelt, D. M., Horowitz, L. W., Naik, V., Golaz, J. C., and Mauzerall, D. L.: Radiative forcing and climate response to projected 21st century aerosol decreases, Atmos. Chem. Phys., 15, 12681–12703, https://doi.org/10.5194/acp-15-12681-2015, 2015.

Wilcox, L., Liu, Z., Samset, B., Hawkins, E., Lund, M., Nordling, K., Undorf, S., Bollasina, M., Ekman, A., Krishnan, S., Merikanto, J., and Turner, A.: Accelerated increases in global and Asian summer monsoon precipitation from future aerosol reductions, Atmos. Chem. Phys., 1–30, https://doi.org/10.5194/acp-2019-1188, 2020.

Wilcox, L., Liu, Z., Samset, B., Hawkins, E., Lund, M., Nordling, K., Undorf, S., Bollasina, M., Ekman, A., Krishnan, S., Merikanto, J., and Turner, A.: Accelerated increases in global and Asian summer monsoon precipitation from future aerosol reductions, Atmos. Chem. Phys., 1-30, https://doi.org/10.5194/acp-2019-1188, 2020.

Wu, G., Baležentis, T., Sun, C., and Xu, S.: Source control or end-of-pipe control: Mitigating air pollution at the regional level from the perspective of the Total Factor Productivity change decomposition, Energy Policy, 129, 1227-1239, https://doi.org/10.1016/j.enpol.2019.03.032, 2019.

Xie, B., Zhang, H., Wang, Z., Zhao, S., and Fu, Q.: A modeling study of effective radiative forcing and climate response due to tropospheric ozone, Adv. Atmos. Sci., 33, 819–828, https://doi.org/10.1007/s00376-016-5193-0, 2016a.

Xie, X., Wang, H., Liu, X., Li, J., Wang, Z., and Liu, Y.: Distinct effects of anthropogenic aerosols on the East Asian summer monsoon between multidecadal strong and weak monsoon stages, J. Geophys. Res. Atmos., 121, 7026–7040, https://doi.org/https://doi.org/10.1002/2015JD024228, 2016b.

Yang, D., Zhao, S., Zhang, H., and Shen, X.Y.: Simulation of global distribution of temporal and spatial variation o f PM2.5 concentration in the future, Zhongguo Huanjing Kexue/China Environ. Sci., 37, 1201–1212, 2017.

You, Q., Wu, F., Shen, L., Pepin, N., Jiang, Z., and Kang, S.: Tibetan Plateau amplification of climate extremes under global warming of 1.5 ℃, 2 ℃ and 3 ℃, Glob. Planet. Change, 192, 103261, https://doi.org/https://doi.org/10.1016/j.gloplacha.2020.103261, 2020.

Zanis, P., Akritidis, D., Georgoulias, K. A., Allen, J. R., Bauer, E. S., Boucher, O., Cole, J., Johnson, B., Deushi, M., Michou, M., Mulcahy, J., Nabat, P., Olivié, D., Oshima, N., Sima, A., Schulz, M., Takemura, T., and Tsigaridis, K.: Fast responses on pre-industrial climate from present-day aerosols in a CMIP6 multi-model study, Atmos. Chem. Phys., 20, 8381–8404, https://doi.org/10.5194/acp-20-8381-2020, 2020.

Zanis, P., Akritidis, D., Turnock, S., Naik, V., Szopa, S., Georgoulias, A., Bauer,S., Deushi, M., Horowitz, L., Keeble, J., Sager, P., O'Connor, F., Oshima, N., Tsigaridis, K., and Noije, T.: Climate change penalty and benefit on surface ozone: a global perspective based on CMIP6 earth system models, Environ. Res. Lett. 17, 024014, https://doi.org/10.1088/1748-9326/ac4a34, 2022.

Zhang, H., Xie, B., and Wang, Z.: Effective Radiative Forcing and Climate Response to Short-Lived Climate Pollutants Under Different Scenarios, Earth's Futur., 6, 857–866, https://doi.org/10.1029/2018EF000832, 2018.

Zhao, A. D., Stevenson, D. S., and Bollasina, M. A.: The role of anthropogenic aerosols in future precipitation extremes over the Asian Monsoon Region, Clim. Dyn., 52, 6257–6278, https://doi.org/10.1007/s00382-018-4514-7, 2018.

Zhao, J., Su, B., Mondal, S. K., Wang, Y., Tao, H., and Jiang, T.: Population exposure to precipitation extremes in the Indus River Basin at 1.5 ℃, 2.0 ℃ and 3.0 ℃ warming levels, Adv. Clim. Chang. Res., 12, 199–209, https://doi.org/10.1016/j.accre.2021.03.005, 2021.

Zheng, B., Tong, D., Li, M., Liu, F., Hong, C., Geng, G., Li, H., Li, X., Peng, L., Qi, J., Yan, L., Zhang, Y., Zhao, H., Zheng, Y., He, K., and Zhang, Q.: Trends in China's anthropogenic emissions since 2010 as the consequence of clean air actions, Atmos. Chem. Phys., 18, 14095-14111, https://doi.org/10.5194/acp-18-14095-2018, 2018.

Zhou, B., and Qian, J.: Changes of weather and climate extremes in the IPCC AR6, Adv. Clim. Chang. Res., 17, 713–718, https://doi.org/10.12006/j.issn.1673-1719.2021.167, 2021

Zhu, X., Lee, S. Y., Wen, X., Ji, Z., Lin, L., Wei, Z., Zheng, Z., Xu, D., and Dong, W.: Extreme climate changes over three major river basins in China as seen in CMIP5 and CMIP6, Clim. Dyn., 57, 1187–1205, https://doi.org/10.1007/s00382-021-05767-z, 2021.

Zhu, X., Lee, S. Y., Wen, X., Ji, Z., Lin, L., Wei, Z., Zheng, Z., Xu, D., and Dong, W.: Extreme climate changes over three major river basins in China as seen in CMIP5 and CMIP6, Clim. Dyn., 57, 1187-1205, https://doi.org/10.1007/s00382-021-05767-z, 2021.

Model	Institution	Country	Atmospheric resolution (Longitude ×Latitude)	realizations
BCC-ESM1	Beijing Climate Centre (BCC)	China	2.81°×2.81°	3
CESM2-WACCM	National Center for Atmospheric Research (NCAR)	United States	1.25°×0.94°	3
GISS-E2-1-G	Goddard Institute for Space Studies (GISS)	United States	2.0°×2.5°	3
GFDL-ESM4	Geophysical Fluid Dynamics Laboratory (GFDL)	United States	1.25°×1.0°	1
EC-Earth3-AerChem	European consortium of meteorological services, research institutes and high-performance computing centers (EC-Earth consortium)	European consortium	0.70°×0.70°	2
MRI-ESM2-0	Meteorological Research Institute (MRI)	Japan	1.87°×1.87°	3
UKESM1-0-LL	Met Office Hadley Centre (MOHC)	United Kingdom	1.88°×1.88°	3

Table 1: [1]**Summary of CMIP6 models used in this study.**

Index Name	Index Definition	Units
The hottest day (TXx)	Annual average of the monthly maximum value of daily maximum temperature	K
The coldest day (TNn)	Annual average of monthly minimum value of daily maximum temperature	K
Warm days (TX90p)	Percentage of days with daily maximum temperature > 90% percentile	%
Warm nights (TN90p)	Percentage of days with daily minimum temperature > 90% percentile	%
Tropical nights (TR)	Annual count of days when daily minimum temperature > 20°C.	days
Warm spell duration (WSDI)	Annual count of days with at least 6 consecutive days when daily maximum temperature > 90th percentile	days
Maximum consecutive 5-day precipitation (RX5day)	Monthly maximum consecutive 5-day precipitation	mm
Total wet-day precipitation (R95p)	Annual total precipitation on days when daily precipitation >95th percentile.	mm
Heavy precipitation days (R10)	Annual count of days when precipitation ≥ 10mm	days
Consecutive dry days (CDD)	The maximum length of dry spell, the maximum number of consecutive days with precipitation < 1mm	days

Table 2: Definitions of the extreme climate indices used in this study.

Models	ERF (W/m^2)	Tas (K)
BCC-ESM1	0.23	0.20
CESM2-WACCM	0.41	0.29
EC-Earth3-AerChem	0.50	0.23
GFDL-ESM4	-0.03	0.24
GISS-E2-1-G	0.19	0.06
MRI-ESM2-0	0.12	0.13
UKESM1-0-LL	0.20	0.22
MMM	0.23	0.19

Table 3. Global effective radiative forcing (ERF) and surface air temperature (SAT) responses to non-methane SLCFs mitigation. MMM is the multi-model mean.

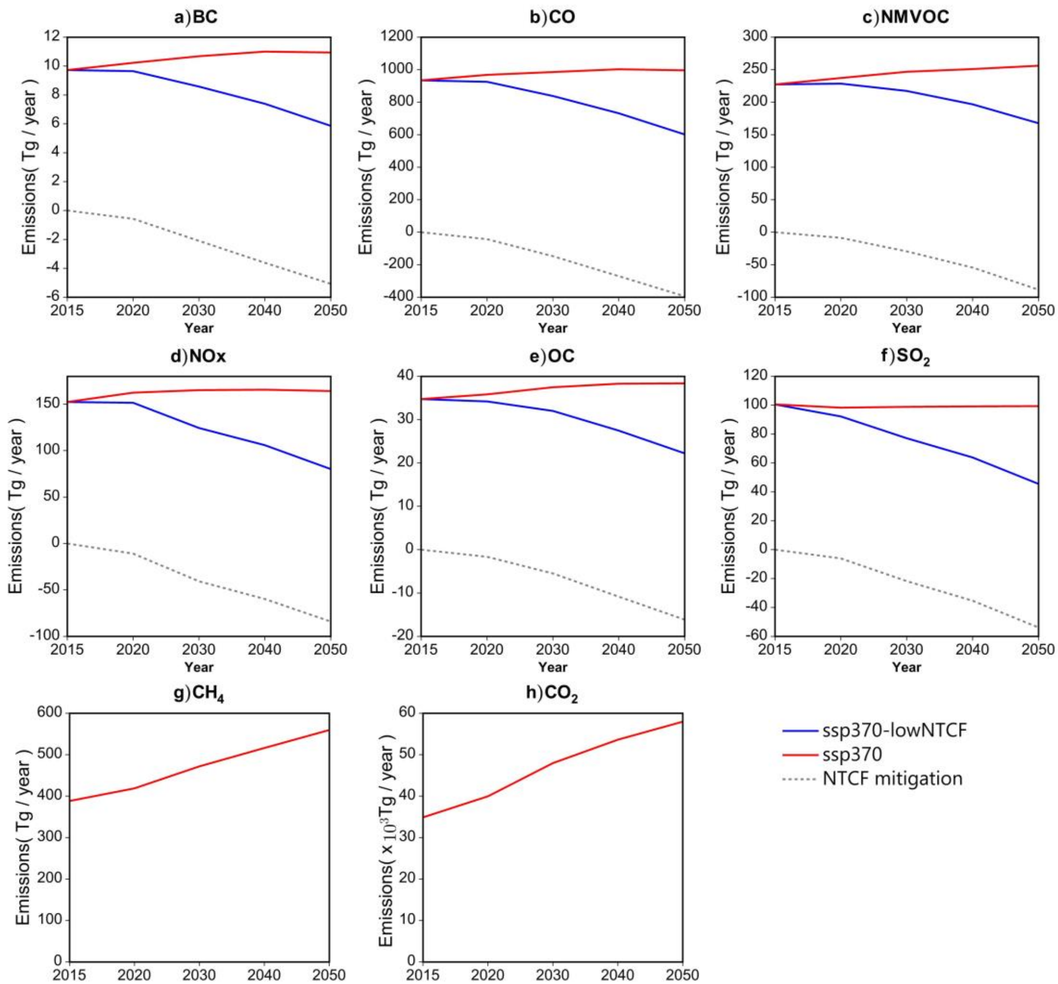

Figure 1: Time series of global annual emissions of (a) BC, (b) CO, (c) NMVOC, (d) NOx, (e) OC, (f) SO_2, (g) CH_4, and (h) CO_2 from 2015-2050 under the SSP3-7.0 (red solid line) and SSP3-7.0-lowNTCF (blue solid line) scenarios. The green dashed lines represent the emission differences between the two scenarios.

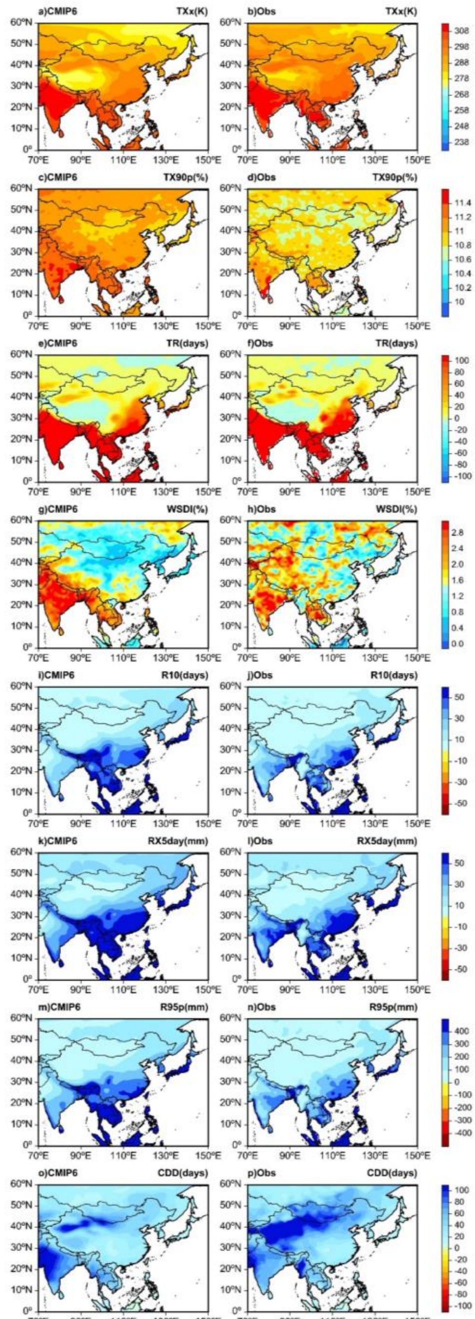

Figure 2: The annual mean of the hottest day (TXx), warm days (TX90p), tropical nights (TR), warm spell duration (WSDI), heavy precipitation (R10), maximum consecutive 5-day precipitation (RX5day), total wet-day precipitation (R95p), and consecutive dry days (CDD) over study area during 1995-2014 for CMIP6 multi-model mean (left column) and gridded observations (right column).

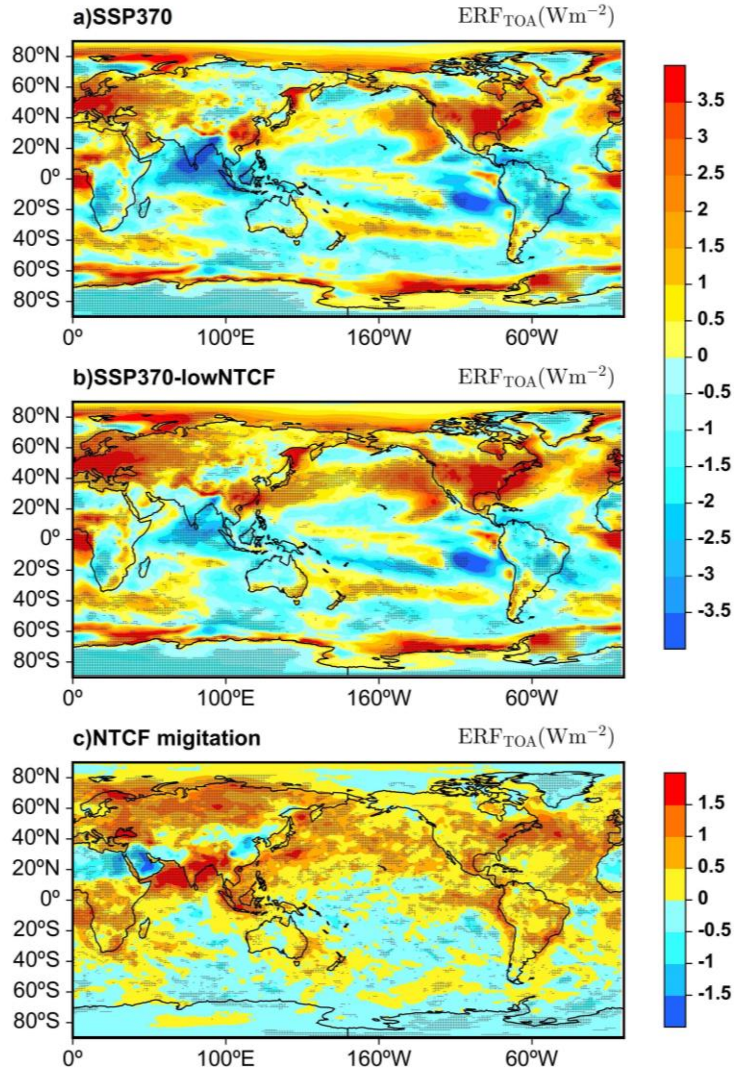

Figure 2: Spatial patterns of effective radiative forcing (ERF) during 2031-2050 under the (a) SSP3-7.0 and (b)SSP3-7.0-lowNTCF scenarios and (c) only caused by the non-methane SLCFs reductions relative to 1995-2014 (units: W m^{-2}). The dotted regions indicate that more than 60% of the models agree on the sign.

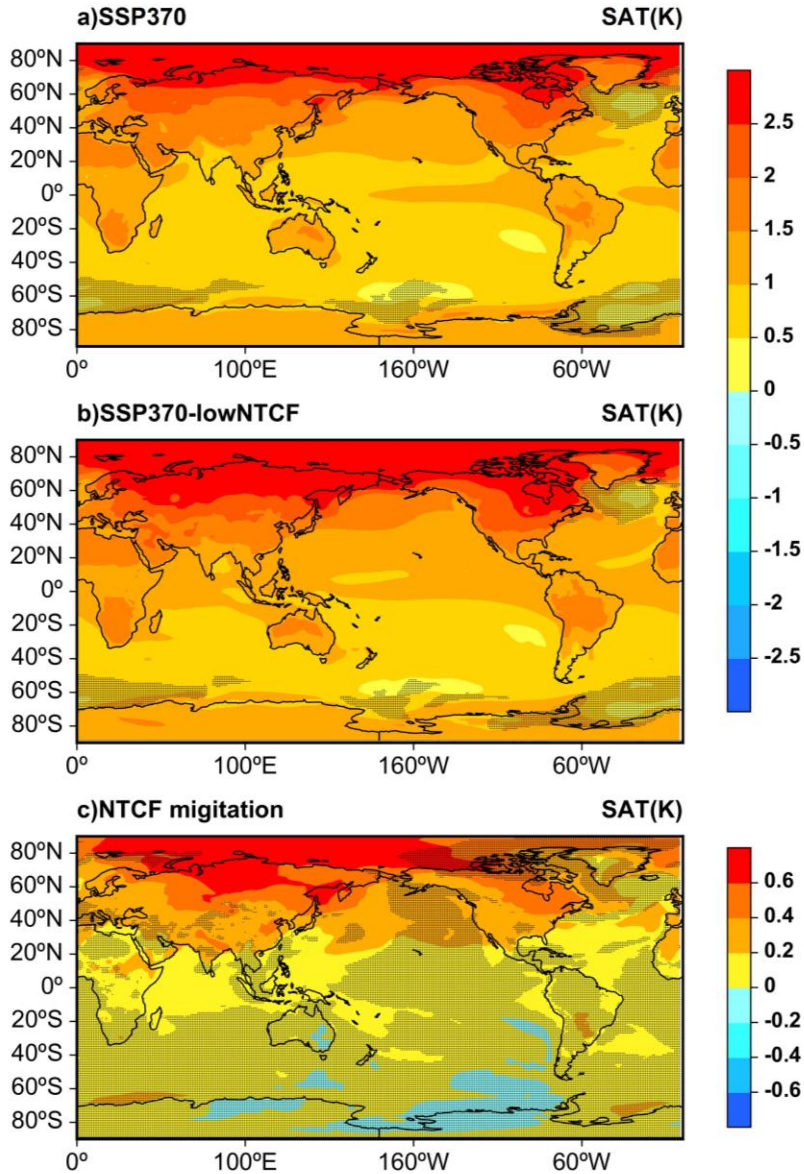

Figure 3: Spatial patterns of changes in surface air temperature (SAT) during 2031-2050 under the (a) SSP3-7.0 and (b) SSP3-7.0-lowNTCF scenarios and (c) only caused by the non-methane SLCFs reductions relative to 1995-2014surface air (units: K). The dotted regions indicate that at least six out of seven models disagree on the sign.

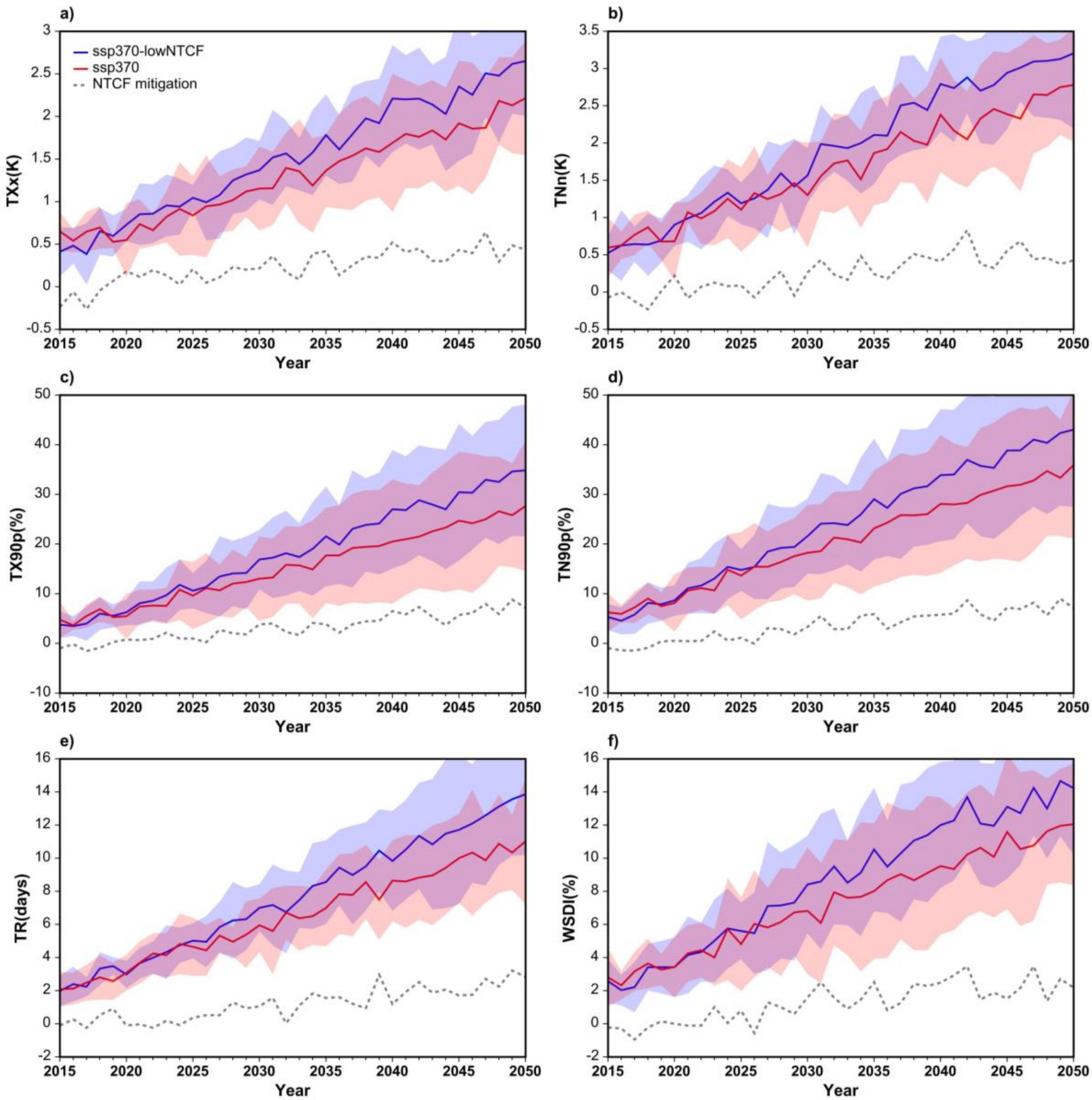

Figure 4: Time series of changes in annual mean the hottest day (TXx), warm days (TX90p), tropical nights (TR), and warm spell duration (WSDI) averaged over Asia under the SSP3-7.0 (red) and SSP3-7.0-lowNTCF (blue) scenarios from 2015 to 2050 relative to 1995-2014. The green dashed lines represent the changes caused by the non-methane SLCFs reductions. The red and blue shading represents two standard deviations across models.

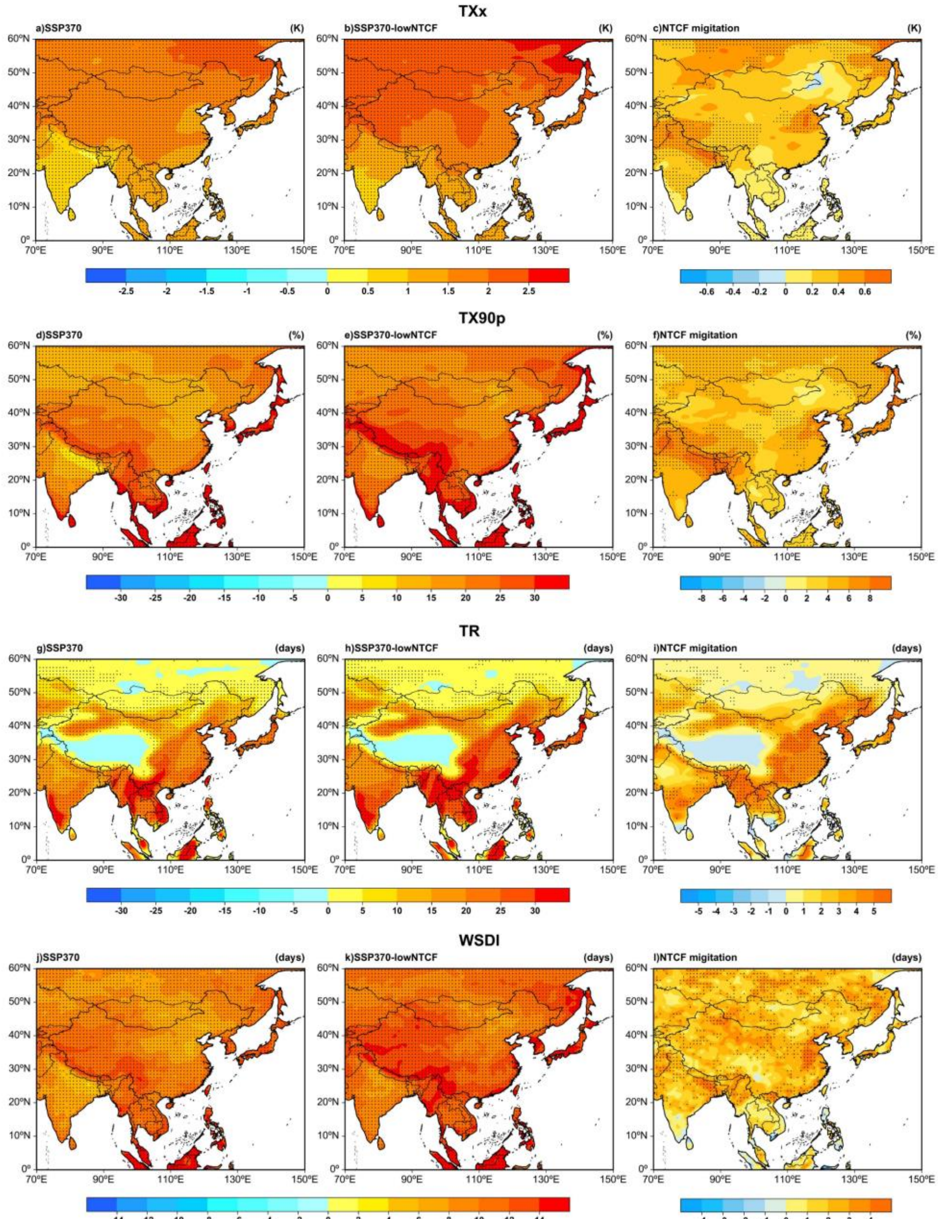

Figure 5: Spatial patterns of changes in the hottest day (TXx), warm days (TX90p), tropical nights (TR), and warm spell duration (WSDI)during 2031-2050 in Asia under the SSP3-7.0 (left column) and SSP3-7.0-lowNTCF (middle column) scenarios relative to 1995-2014. The right column represents changes caused by the non-methane SLCFs mitigation. The dotted regions indicate that at least four out of five models agree on the sign.

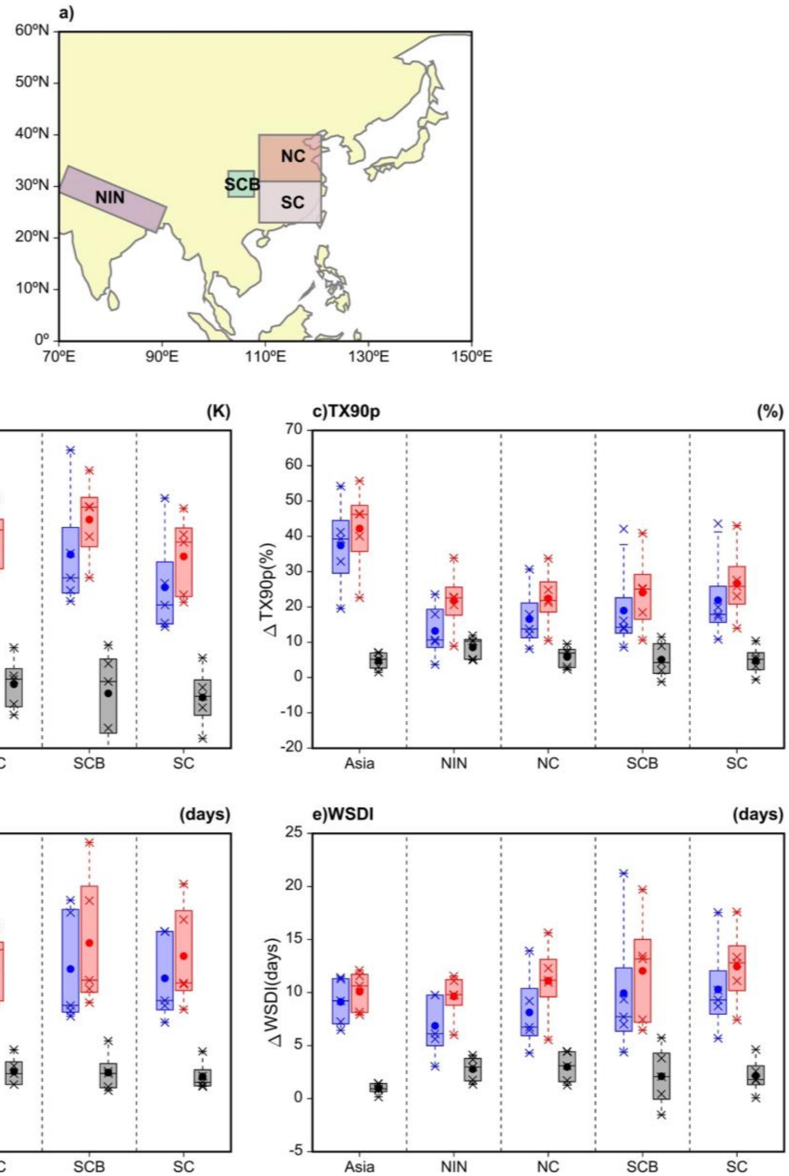

Figure 6: Changes in the hottest day (TXx), warm days (TX90p), tropical nights (TR), and warm spell duration (WSDI) averaged over NIN, NC, SC, and SCB during 2031-2050 relative to 1995-2014 under the SSP3-7.0 (red) and SSP3-7.0-lowNTCF (blue) scenarios. The gray bars represent the changes caused by the non-methane SLCFs reductions. The star symbols indicate the individual models, and the boxes indicate the spread from the 25th to the 75th percentile of the models, with the center lines representing the median and the dot representing the mean values.

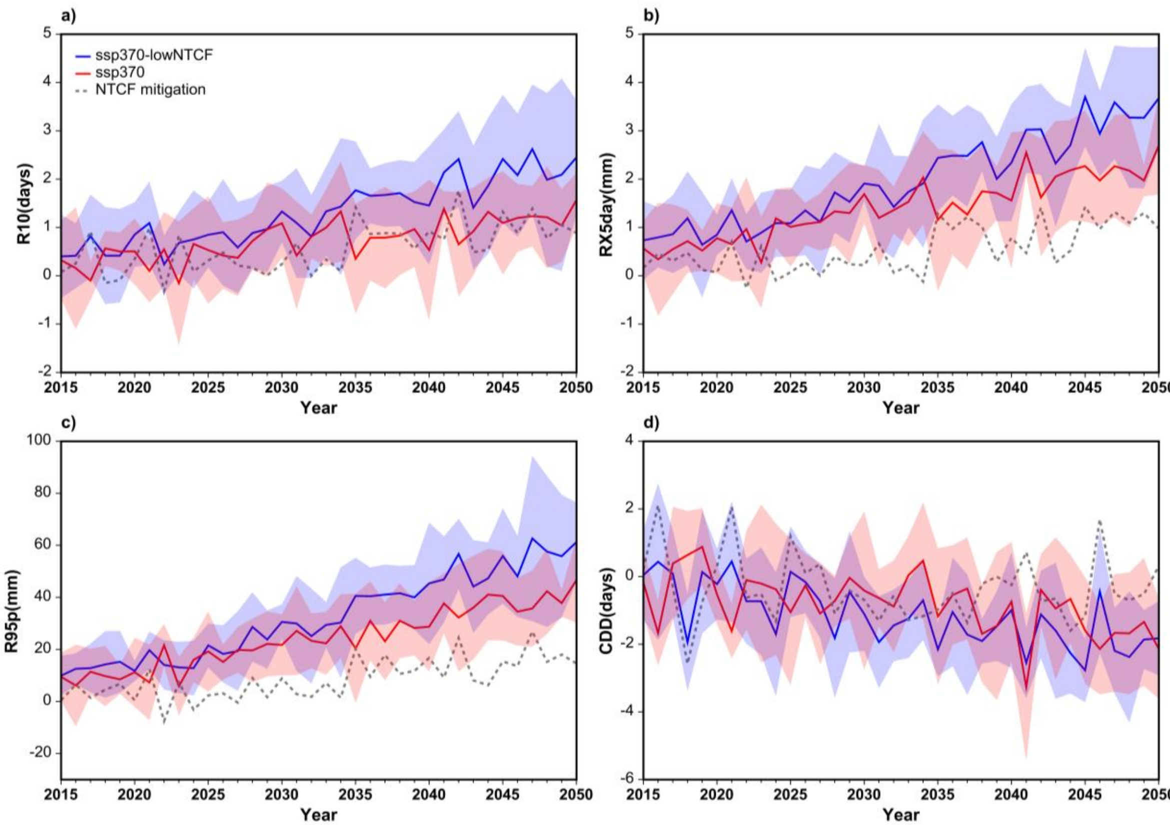

Figure 7: Time series of changes in annual mean heavy precipitation (R10), maximum consecutive 5-day precipitation (RX5day), days, total wet-day precipitation (R95p), and consecutive dry days (CDD) averaged over Asia under the SSP3-7.0 (red) and SSP3-7.0-lowNTCF (blue) scenarios from 2015 to 2050 relative to 1995-2014. The green dashed lines represent the changes caused by the non-methane SLCFs reductions. The red and blue shading represents two standard deviations across models.

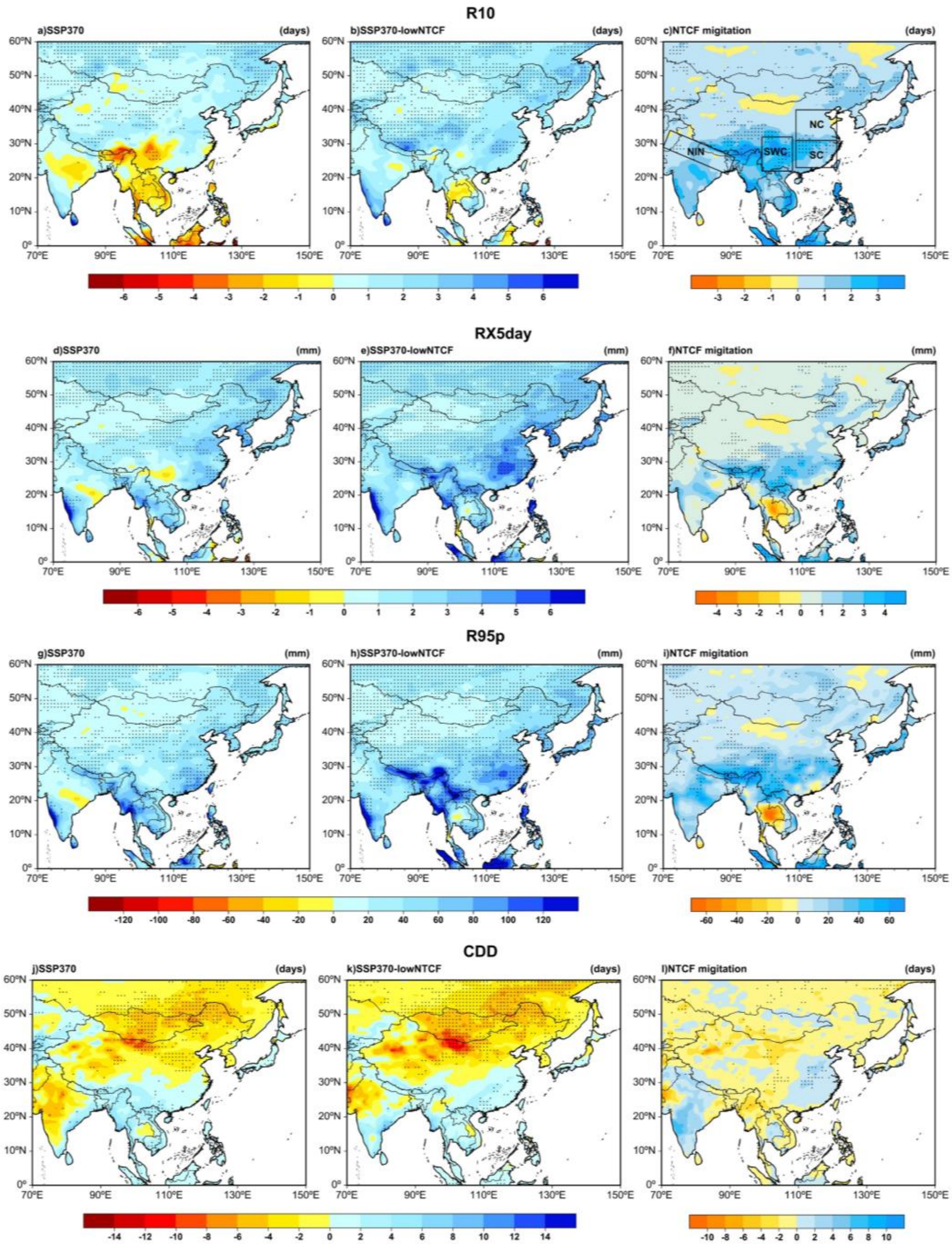

Figure 8: Spatial patterns of changes in heavy precipitation (R10), maximum consecutive 5-day precipitation (RX5day), days, total wet-day precipitation (R95p), and consecutive dry days (CDD) during 2031-2050 in Asia under the SSP3-7.0 (left column) and SSP3-7.0-lowNTCF (middle column) scenarios relative to 1995-2014. The right column represents changes caused by the non-methane SLCFs mitigation. The dotted regions indicate that at least five out of six models agree on the sign.

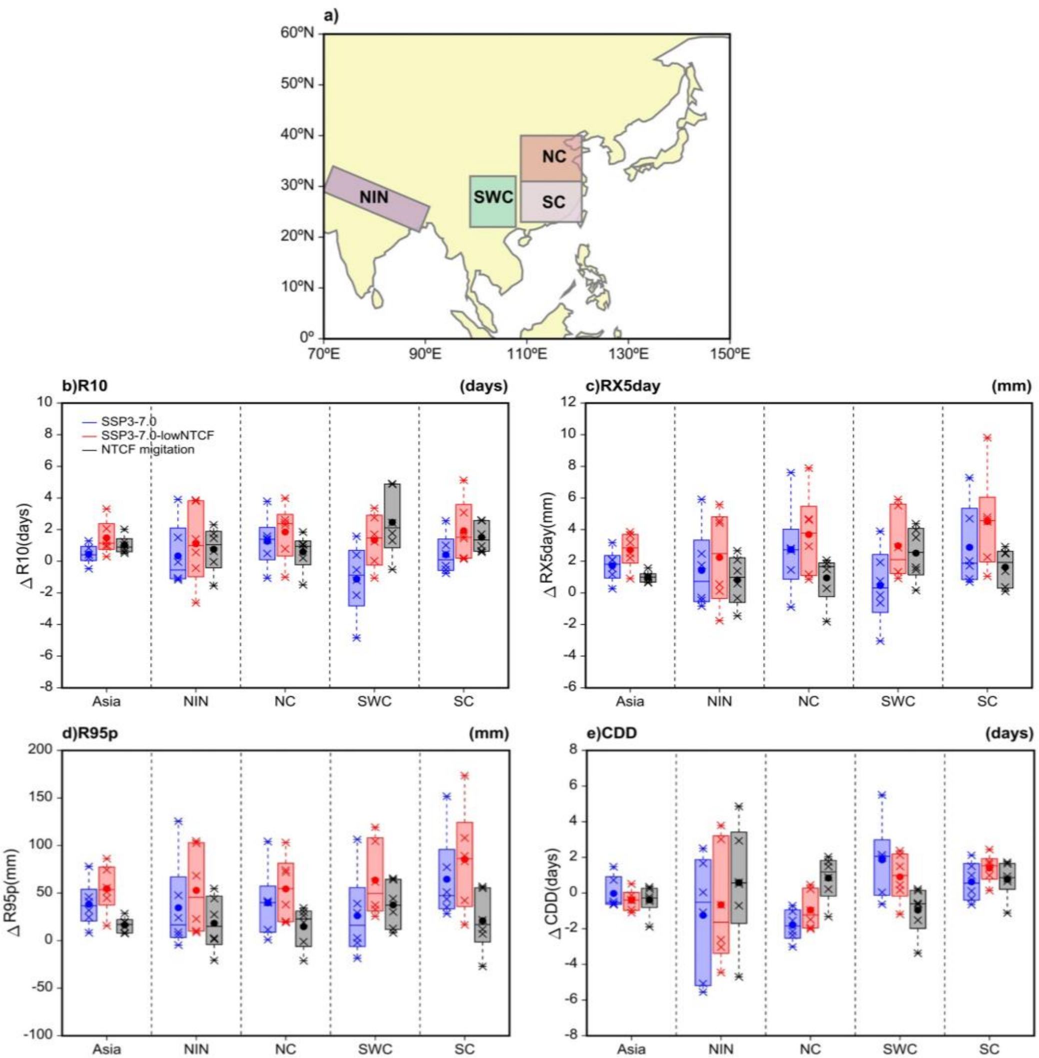

Figure 9: Changes in heavy precipitation (R10), maximum consecutive 5-day precipitation (RX5day), days, total wet-day precipitation (R95p), and consecutive dry days (CDD) averaged over NIN, NC, SC, and SCB during 2031-2050 relative to 1995-2014 under the SSP3-7.0 (red) and SSP3-7.0-lowNTCF (blue) scenarios. The gray bars represent the changes caused by the non-methane SLCFs reductions. The star symbols indicate the individual models, and the boxes indicate the spread from the 25th to the 75th percentile of the models, with the center lines representing the median and the dot representing the mean values.

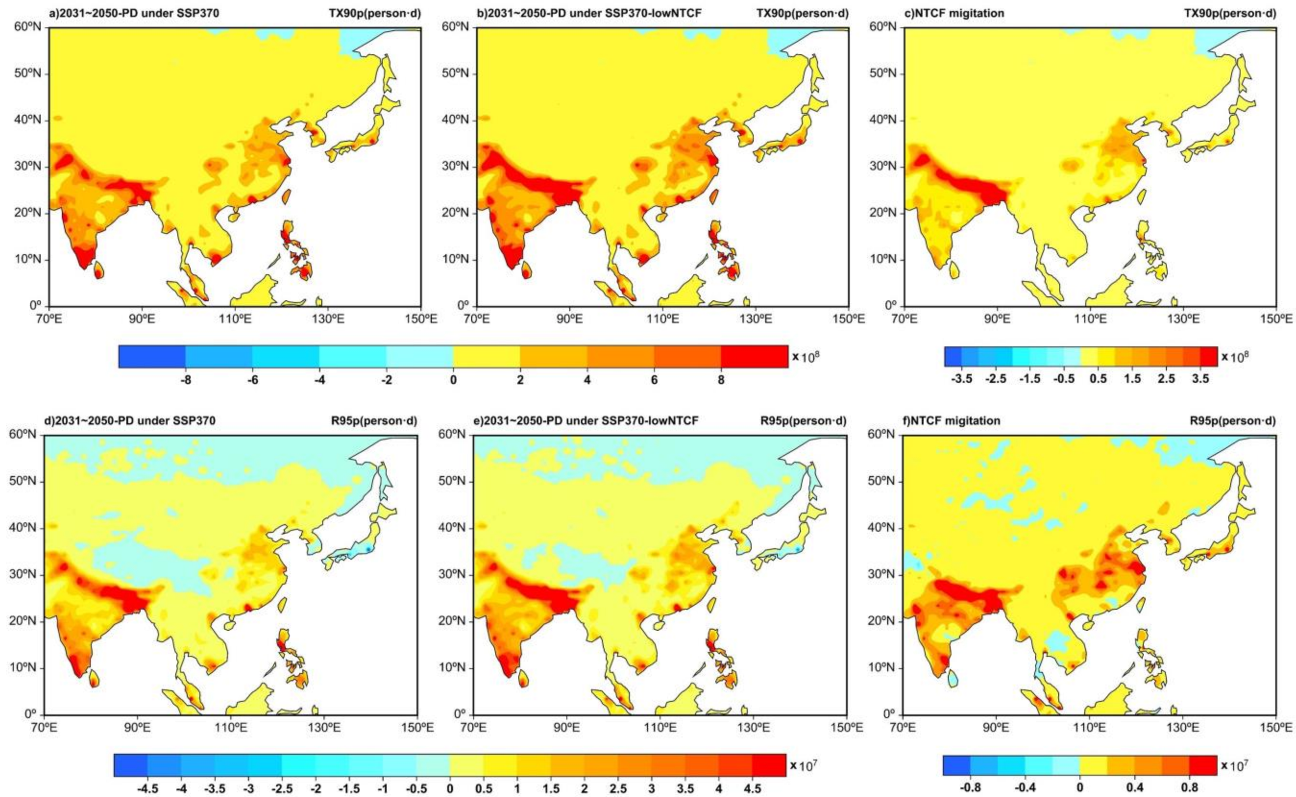

Figure 10: Spatial patterns of changes in population exposed to warm days (TX90p) and total wet days (R95pdays) in Asia during 2031-2050 under the SSP3-7.0 (left) and SSP3-7.0-lowNTCF (middle) relative to 1995-2014 (units: person-days). The right column represents the changes caused by the non-methane SLCFs reductions.

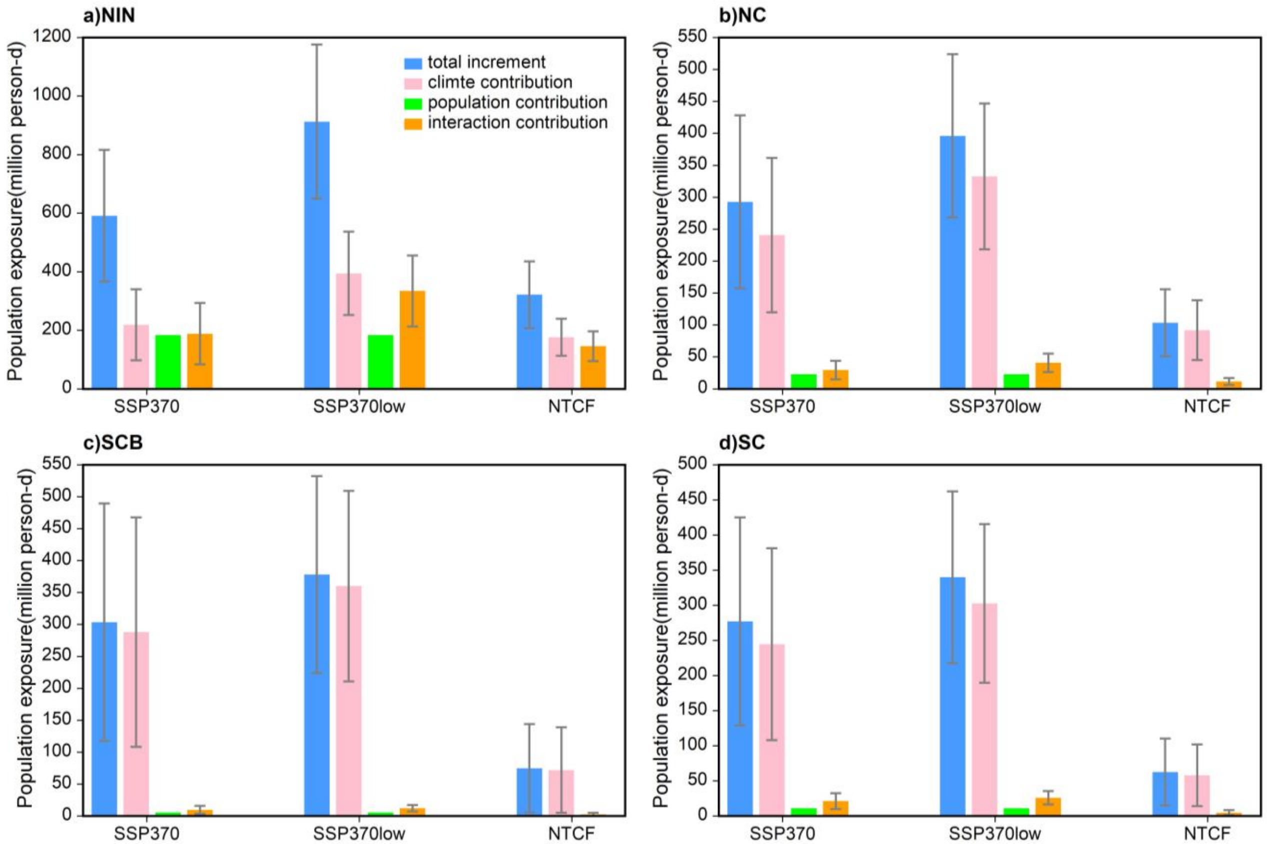

830 **Figure 11: The total changes of population exposure to warm days (TX90p) averaged over different regions under the SSP3-7.0 and SSP3-7.0-lowNTCF scenarios and its changes driven by the non-methane SLCFs reductions. The blue, yellow, and red bars represent the changes driven by climate change, population change, and population-climate interaction, respectively. The error bars denote two standard deviations across models.**

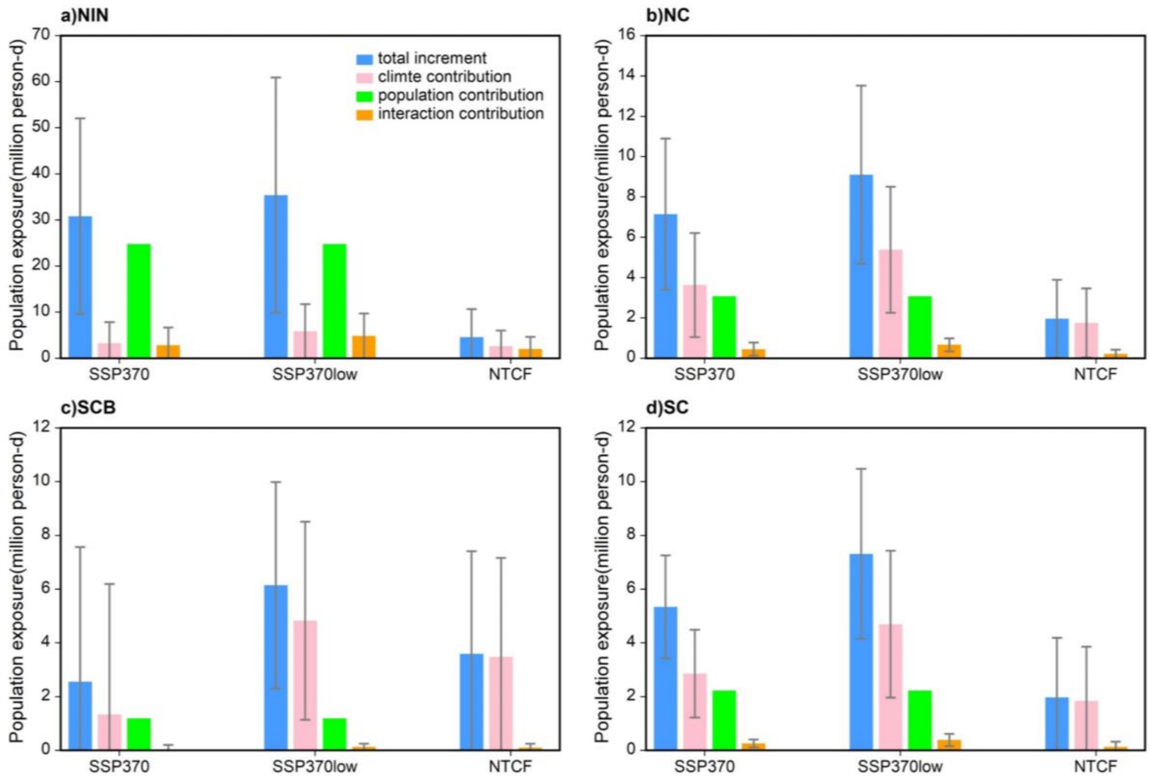

835 **Figure 12: The total changes of population exposure to wet days (R95pdays) averaged over different regions under the SSP3-7.0 and SSP3-7.0-lowNTCF scenarios and its changes driven by the non-methane SLCFs reductions. The blue, yellow, and red bars represent the changes driven by climate change, population change, and population-climate interaction, respectively. The error bars denote two standard deviations across models.**